HIGH DYNAMIC RANGE INFRARED RADIOMETRY AND IMAGING

FINAL REPORT

Contract Number NAS5-30282

Microtronics Associates
4516 Henry Street, Suite 403
Pittsburgh, PA 15213
(412) 681-0888

The purpose of the Phase I research entitled "High Dynamic Range Infrared Radiometry and Imaging" was the development of cryogenic extrinsic silicon infrared (IR) detector systems which perform intensity-to-frequency conversion at the focal plane via simple circuits with very low power consumption. The incident IR intensity controls the repetition rate of short duration output pulses over a pulse rate dynamic range of about 10^6. Pulse heights are typically greater than 1 volt so that no preamplifiers are required. Each detector can drive a separate LED so that pulse coded image data can be optically transmitted out of the cryogenic environment. Pulse timing or counting provides an accurate means of signal coding and digitization. Measurements of pulse rate as a function of intensity over the full dynamic range were carried out and compared with our theoretical model. Theory indicates the possibility of monotonic and approximately linear response over the full dynamic range. A comparison between the theoretical and the experimental results shows that the model provides a reasonably good description of experimental data. Some measurements of survivability with a very intense IR source were made on these devices and found to be very encouraging. A preliminary investigation of impurity band impact ionization as a means of achieving increased sensitivity has been carried out. This possibility appears reasonable because of recent successful work on infrared photomultipliers.

Evidence continues to indicate that some variations in interpulse time intervals are deterministic rather than probabilistic. This indicates that nonlinear dynamics concepts may give rise to a new means of low noise IR detection.

Systems employing the detectors studied in Phase I would be useful in many infrared radiometric and imaging applications, including simultaneous measurement of astrophysical source luminosities ranging over many orders of magnitude. It is highly desirable to be able to tailor the dynamic range to correspond to anticipated ranges of intensity. Phase I modeling efforts represent a significant step in this direction because the modeling provides a quantitative link between device parameters and the dynamic range. The ultralow power associated with our approach and the novel aspects of IR intensity-to-frequency conversion could lead to entirely new means of focal plane processing as well as high dynamic range radiometry and imaging.

1 Overview

The research described herein involves the use of cryogenically cooled, extrinsic silicon infrared detectors in an unconventional mode of operation which offers an unusually large dynamic range. The use of these detectors for high dynamic range IR radiometry and IR imaging would require **no preamplifiers** and could open the way to new means of processing at or near the focal plane. The detectors perform intensity-to-frequency conversion via circuits with very low power consumption. Many accurate means of measurement are based on the conversion of an analog input signal to a frequency which can be accurately measured. To our knowledge, our approach is the only one which is based on direct IR intensity-to-frequency conversion in the detector itself.

There are many situations in which a high dynamic range is useful simply by the nature of the application. For example, the luminosities of astrophysical sources vary over many orders of magnitude.[1,2,3] Measurements of high radiometric fidelity are complicated whenever the range of luminosity exceeds the dynamic range of the detector system. Simultaneous measurement of very bright and very dim sources may be ruled out and lack of simultaneity becomes especially unfortunate if temporal changes in the image are possible.

There are also situations in which the presence of a bright object in the field of view causes saturation problems which prevent the observation of dim objects. If clock rates (integration times) of scanned or synchronized readout systems are changed to accommodate bright objects then the integration time needed for dim objects is diminished. In the proposed system there is no synchronization. Each detector produces output pulses at a rate determined by the incident infrared flux it sees. (Our model of this is included below.) Each detector and its associated RC load can be thought of as an asynchronous integrate-and-fire IR detector.[4]

The spectral response of these detectors has been measured[5,6] with a liquid-helium-cooled monochromator and found to be similar to other extrinsic detectors[7,8,9,10] employing the same impurity. Therefore, we expect that conventional extrinsic detectors with particular impurities which are currently used in particular wavelength ranges could be replaced by injection mode detectors operating over the same wavelength ranges.

Low power consumption and simple circuitry will facilitate highly parallel readout. Parallel transfer of data from a focal plane array to a processor could eliminate the need for multiplexing at the focal plane. In our approach, the IR detector output consists of fast pulses which are of sufficient amplitude to drive LEDs. It is not necessary to use LEDs and optical readout since direct electrical readout is possible. However, pulsed LED techniques could provide an efficient means of data transfer out of a cryogenic environment with an extremely low heat load.

The spontaneous generation of pulses in silicon p^+-n-n^+ diodes at liquid helium temperatures has been studied extensively.[5,11,12,13,14] The simple circuit used to obtain

these pulses (Fig. 1) consists of a p^+-n-n^+ diode and a load resistor, a capacitance and a power supply. The incident IR intensity controls the pulse repetition rate over a pulse rate dynamic range of about 10^6. Pulse heights are typically in the range 1 volt to 50 volts which eliminates the need for preamps. The high pulse height and the fast rise time (typically under 100 nanoseconds) of these pulses gives a very high slew rate[13]. Hence, the time intervals between pulses can be measured accurately. Time interval measurements represent an alternative to pulse counting as means of readout. In some instances, measurements of each successive time interval (time series) can convey more information than the mean pulse rate. Our previous time series studies have revealed some remarkable results[14] involving nonlinear dynamics and mode locking and lead to minimum resolvable temperatures of 0.01K.

2 High Dynamic Range Measurements

2.1 Apparatus and Instrumentation

Figure 2 and Fig. 3 show the experimental setup used in the measurement of dynamic range. This apparatus was designed and built by Microtronics Associates. The apparatus is used as an insert in a liquid helium storage dewar in order to conserve liquid helium by avoiding helium transfer. In operation, the detector and the filter assembly are submerged in liquid helium, while the heater, i.e. the infrared source, is above the liquid helium level. Three commercial neutral density filters with transmission of about 0.01 (from Infrared Laboratories) were used to obtain a dynamic range of about 10^6. The three filters were in filter holders whose position can be controlled from outside the dewar by means of the actuator rods. See Fig. 3. Each filter can independently moved in or out of the optical path so that the IR beam will pass through none, one, two or all three filters. The IR source is a heater coil made of manganin.

The CAMAC data acquisition system used in many of our Phase I experiments is shown in Fig. 4. The advantage of a CAMAC system is that it is both powerful and flexible. Many different input and output tasks can be incorporated by inserting appropriate

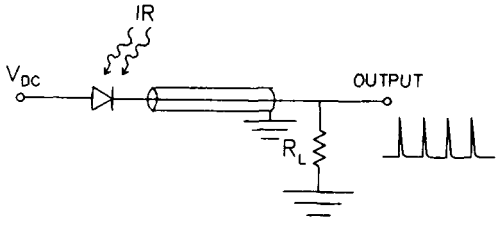

Figure 1: Circuit diagram showing a dc forward biased p^+-n-n^+ diode and the pulse output. The load impedance consists of R = 50K Ω and C = 200 pF. This simple circuit eliminates the need for a preamplifier and it performs IR intensity-to-frequency conversion.

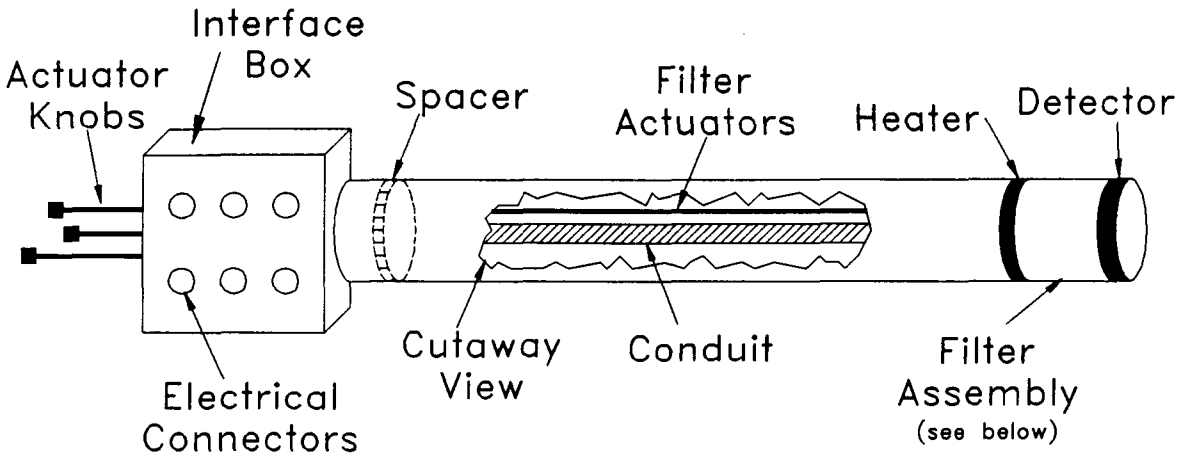

Figure 2: The experimental setup used to measure dynamic range. Electrical connections are for the detector and for the heater. In operation, the detector and filter assembly are in liquid helium while the interface box is outside the helium dewar. Actuator rods control the positioning of the filters. A blowup in Fig. 3 shows the filter holder assembly. The filter assembly and detector mounting are made of thick aluminum for good electrical shielding and good radiation shielding. The remainder of the unit is made mainly of thin wall (seamless) stainless steel and small diameter steel rods in order to reduce heat flow into the dewar.

CAMAC modules. The system is easily reconfigured and reprogrammed.

2.2 Experimental Results

Some initial measurements revealed problems at the low intensity end of the dynamic range measurements due to IR radiation leaks when filter carriers were moved out of the IR beam. When the heater source was off and one of the filter carriers was out of the optical path, the detector was sensitive enough to detect infrared radiation from the top of the dewar, scattered through the filter carrier slot and again scattered in the direction of the detector. To avoid this side illumination of the filter carrier slots, the filter assembly was surrounded with several layers of aluminum foil. The absence of penetration of IR radiation was verified by comparing the detector signal with the heater off and filter carriers in or out of their slots.

The data in Fig. 5 show that the detector is sensitive to IR over a range of intensities of about 10^6. The heater on-off ratio when all three filters are in the IR path is about 6. That is the frequency is 1.9×10^{-3} Hz with heater off and 1.2×10^{-2} Hz with heater on. This shows that there is measurable response at the low end of the intensity range despite the approximately 10^6 attenuation. In other words, there is a pulse rate which is distinguishable from a dark pulse rate. The approximately linear character of the data plotted in Fig. 5 agree with the model discussed below.

We have considered the possibility that deviations from perfect neutral density filter behavior might cause some deviations from anticipated results. If one portion of the IR

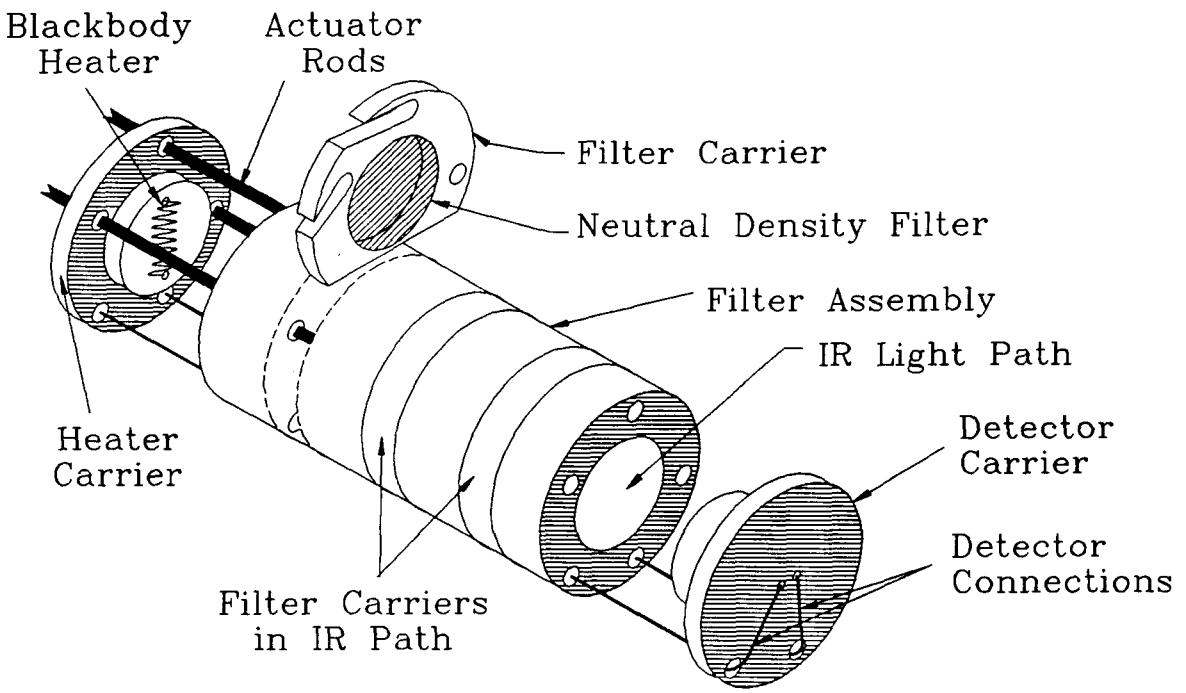

Figure 3: Filter holder assembly showing one filter out of the IR path and the other two filters in the IR path. Three actuator rods rotate three filter carriers in and out of the optical path. This motion requires that each carrier have a different and special shape which provides clearance around rods attached to the other filter carriers and which permits the filter assembly to remain topologically connected. The highly unique shapes were machined by Microtronics Associates using a computer controlled milling machine. Infrared radiation from the heater passes through 0, 1, 2, or 3 filters in the filter assembly and is then detected by a detector mounted on the detector carrier.

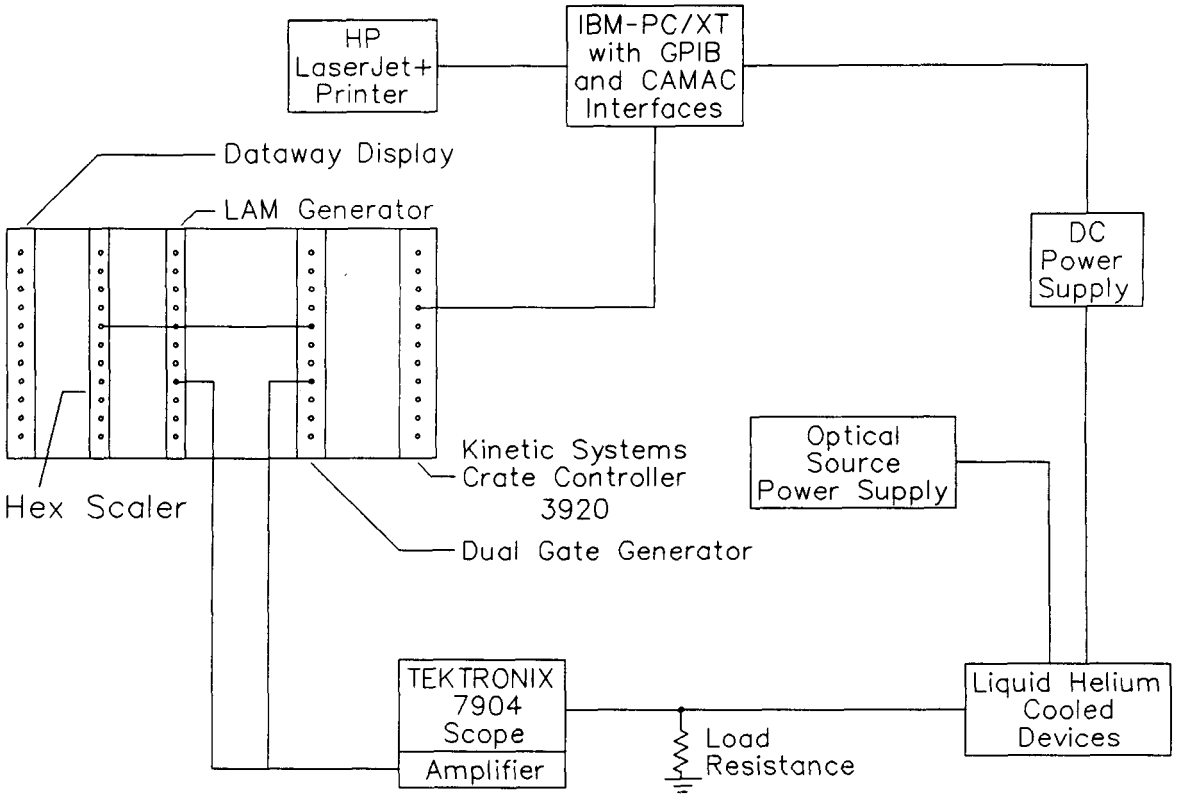

Figure 4: Block diagram showing the electronics used to measure time intervals between successive pulses and the number of pulses in a given time interval. Simultaneous pulse counting can be used as an independent check on the number recorded and digitized time intervals. Counting is much faster than time interval measurement, so that it provides a good check that two pulses have not arrived in quick succession and been missed by the time interval digitizer.

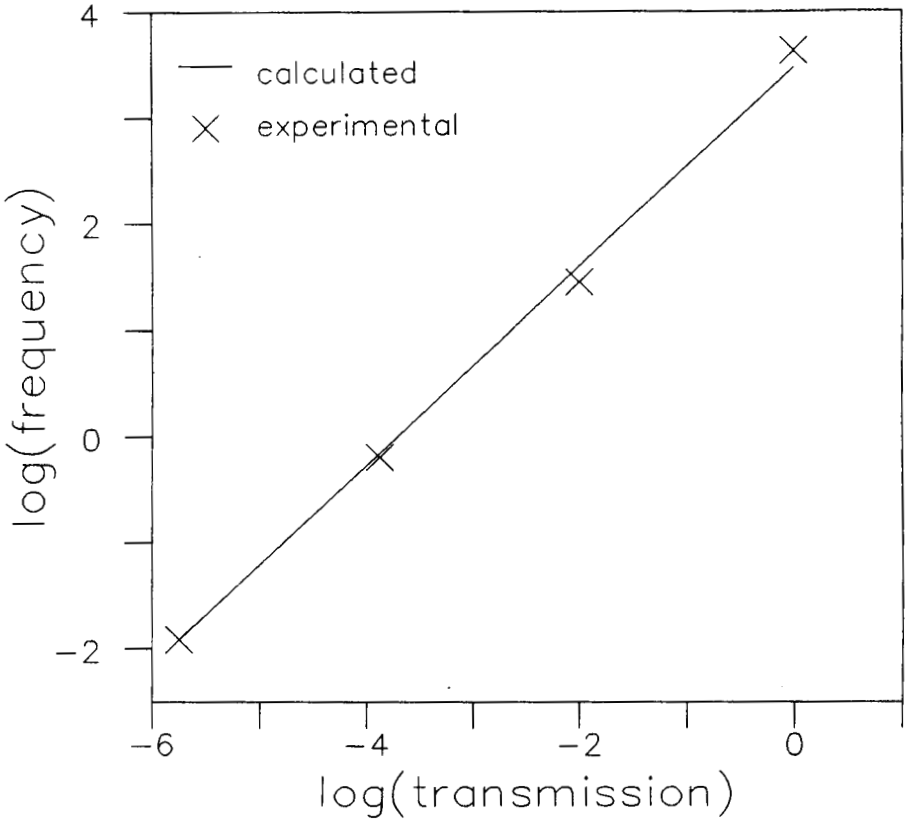

Figure 5: Base 10 logarithm of the pulse rate vs incident IR flux (transmission) with unit flux (logarithm zero) representing the flux incident on the detector without any filters in the IR optical path. The detector bias voltage was 14.6 volts and the dark pulse rate was 1.9×10^{-3} Hz.

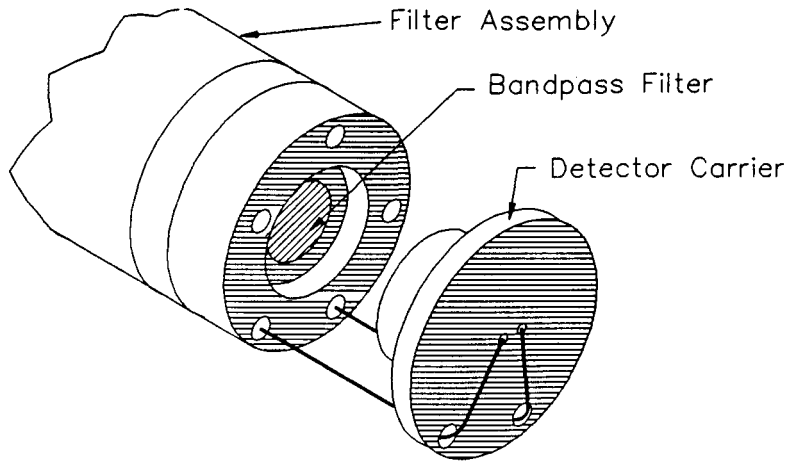

Figure 6: Modification done on the filter assembly to include the band pass filter.

spectrum is attenuated more than another portion of the IR spectrum, then the result will be curvature in Fig. 5. For this to occur, the aforesaid portions of the IR spectrum must overlap the range of wavelengths in which the detector responds. The neutral density filters are made of Si and nichrome powder and we have found that they possess some structure around 20 microns which is within the sensitive range of the detector. We have therefore modified the experimental apparatus (see Fig. 6) to include a bandpass filter in order to block the wavelength around 20 microns.

With this arrangement, the data in Fig. 7 were obtained.

2.3 Correction for Filter Reflectance.

We have derived a formula to take into account the reflectivity of the filters since with more than one filter in the beam, multiple reflections can increase the beam intensity somewhat. The formula for the transmitted beam after passing through three filters is

$$T_1 \times \frac{T_2}{1-R^2} \times \frac{T_3}{1-R^2}$$

where T_1, T_2 and T_3 are the transmission coefficients of the three filters (0.01 in our case) and R is the reflection coefficient of the filters, which is 0.3 for our filters because they are made of silicon. This result is used in Figs. 5,7 and 8.

3 Modeling of Detector Response

In the presence of IR radiation, the space charge buildup in the detector i-region (see Fig.9) is described by

$$\frac{d\rho}{dt} = n\sigma_i\, j + \frac{e\sigma_p n I}{h\nu} \qquad (1)$$

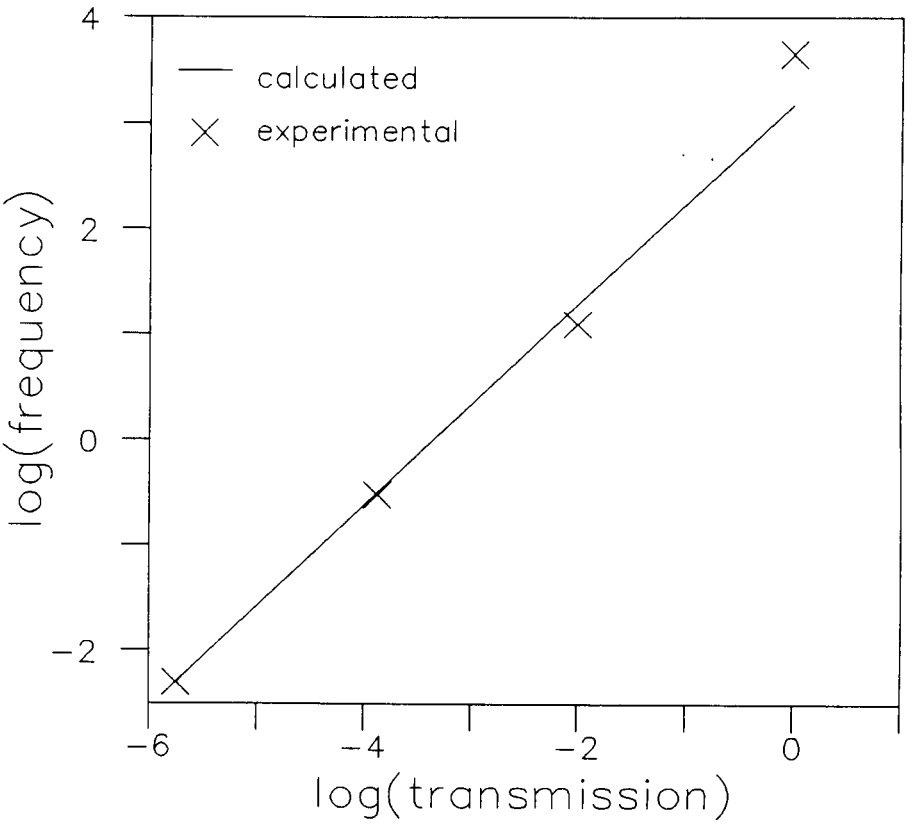

Figure 7: The detector output as in Fig. 5 except for the bandpass filter in the infrared path in order to block the infrared flux around 20 microns.

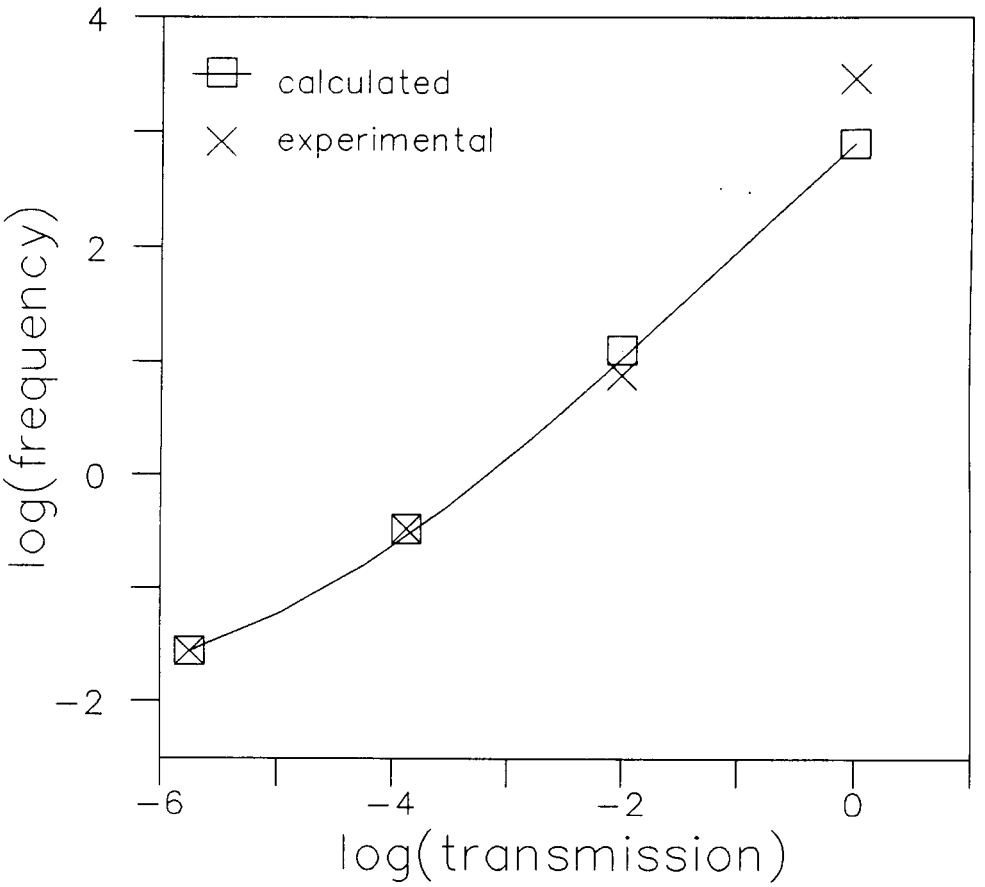

Figure 8: The detector output for lower blackbody temperature which is around 100K. This data set shows much more curvature than the other two, which agrees with the model.

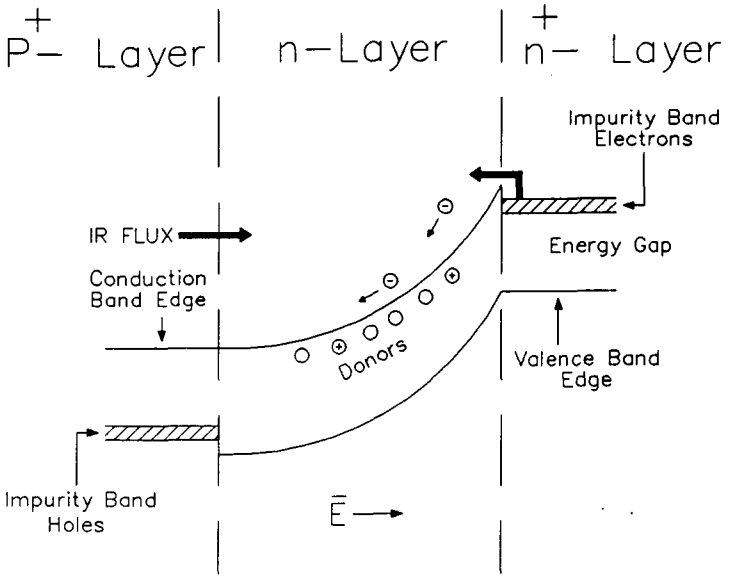

Figure 9: Band diagram of a forward biased p^+-n-n^+ diode at low temperatures. Carriers remain trapped in n-region phosphorus impurities until photoionization or impact ionization occur. Excited carriers are swept out by the electric field. Fermi levels in the p^+ and n^+-layers are offset from the valence and conduction-band edges due to the formation of impurity bands.

where σ_i is the impact ionization cross section, [15,16] σ_p is the photoionization cross section,[17] and n is the concentration of unionized traps. I is the intensity of the source, $h\nu$ is the energy of the IR photon and ρ is the space charge density. The first term corresponds to IR photoionization and the second term corresponds to impact ionization. From Gauss's law, the field at the n^+-n interface is given by

$$F = \frac{(V - V_0)}{D} + \frac{1}{D\epsilon}\int_0^D x\rho(x)dx, \tag{2}$$

where V is the voltage across the diode, D is the i-region thickness and V_0 accounts for the Fermi level difference between the p and n impurity bands. For simplicity, we assume that the space charge is uniform over the diode thickness.

The Richardson-Dushman equation for the injection current density[18] becomes

$$j = A^*T^2 e^{-(\Delta - edF)/kT} \tag{3}$$

Combining the above equations, we get

$$j(t) = \frac{bc}{n\sigma_i[(c + be^{-a\rho_0})e^{-abt} - c]} \tag{4}$$

where $c = n\sigma_i A^*T^2 \exp(-\Delta + ed(V - V_0)/D)/kT$, $b = \sigma_p nIe/h\nu$, and $a = edD/2\epsilon kT$.

From the above equation, we see that the firing occurs when
$[c + b\exp(-\rho_0)]\exp(-abt) = c$ which gives

$$f = f_{dark} \frac{I/I_0}{\ln(1 + I/I_0)} \tag{5}$$

where

$$f_{dark} = \frac{edDc}{2\varepsilon kT} \exp(a\rho_0) \tag{6}$$

and

$$\frac{1}{I_0} = \frac{e\sigma_p \exp(-a\rho_0) \exp(\Delta/kT)}{h\nu\sigma_i A^* T^2 \exp[ed(V - V_0)/DkT]}$$

or

$$\frac{1}{I_0} = \frac{2\varepsilon kTn\sigma_p \exp(-a\rho_0)}{f_{dark} dDh\nu}$$

Current responsivity (R) is given by q df/dI, where q is the charge per pulse, df is the change of frequency of the output pulse rate and dI is the change of incident IR flux. This has been observed to be 9.2 A/W or 9×10^9 Hz/W with power incident on the diode being 2×10^{-2} W/m^2. For high intensities (i.e. $I/I_0 >> 1$) the frequency responsivity df/dI becomes

$$\frac{df}{dI} = \frac{f_{dark}}{I_0} \frac{\ln(I/I_0) - 1}{[\ln(I/I_0)]^2}$$

Noise equivalent power is given by $A(dI/df)(\delta f)$, where A is the area of the device, (dI/df) is the frequency responsivity, and δf is the variation of the dark pulse rate. Specific detectivity (D^*) can be obtained from noise equivalent power. For example, for a particular (nonoptimized) detector at 16.5 V bias, we observe a dark pulse rate of 0.14 Hz over a 50-second interval with a $\delta f = 0.005$ Hz which corresponds to $D^* = 3 \times 10^{12}$ cm Hz$^{1/2}$ W^{-1} for the 27 μm region, where the detector has its highest sensitivity. For comparison with other published results, we note that the blocked-impurity-band (BIB) detectors[19] of Rockwell have a D^* of about 6×10^{12} cm Hz$^{1/2}$ W^{-1} and a responsivity of 6.5 A/W.

4 Comparison of Modeling with Experimental Results

The graphs in Figs. 5 and 7 show the comparison between the experimental results and the calculated results from our model. The data show some deviation from the model. Because we have only three filters, the data points are limited to only four points. In both the curves the third (i.e. one filter in the IR path) and fourth (i.e. no filters in the IR path) experimental points deviate from the calculated points. The third calculated point is a little higher than the experimental point while the fourth point is lower than the experimental point. It is too early to conclude that the model needs some adjustment,

because we have seen the detector is extremely sensitive to scattered radiation. Even inside the storage dewar we have seen the detector responding to radiation from the top of the (inside) dewar, even with one sheet of aluminum foil around the detector assembly. Some residual scatter might explain the fourth point being higher than the expected value, but the third point goes in the other direction. For the calculated values in Fig. 5, f_{dark} is 5.2 $\times 10^{-6}$ Hz and I/I_0 is 2.35 $\times 10^4$. For Fig. 7 the values were 9.6×10^{-9} Hz and 8.25 $\times 10^6$ respectively. In both cases the blackbody temperature was around 225K.

Fig. 8 shows the same comparison for a data set obtained with a lower blackbody temperature of around 100K. In this data set, the experimental points show a larger curvature than in the previous two sets. This agrees with the model, for at lower intensities the model tends to show some curvature. For data in Fig. 8, f_{dark} is 1.9×10^{-2} Hz and I/I_0 is 1.01. The heater on-off ratio when all three filters are in the IR path is about 1.5. That is, the frequency is 1.9×10^{-2} Hz with heater off and 2.7×10^{-2} Hz with heater on. Note that the calculated and observed dark rates match very closely.

5 Pulse Rate Variations and Means of Noise Reduction

We have analyzed pulse rate variations in order to gain a better understanding of noise issues. We continue to see evidence for some remarkable effects which we observed earlier.[13,14] For many diodes, as the bias voltage is adjusted, we find ranges of bias voltage in which the pulsing is more nearly periodic than in other ranges. Nearly periodic pulsing corresponds to low noise. The points discussed in Ref. [13], Ref. [14] and Appendix 1 strongly indicate that most of the pulse interval variations seen to date are deterministic rather than probabilistic so that they do not represent noise in a fundamental sense.

The distinction between deterministic fluctuations and probabilistic fluctuations is one that is made in the literature on chaos, mode locking and nonlinear dynamics. In connection with the detectors described here, it appears that there is an opportunity to bring the results and concepts of research on nonlinear dynamics to bear on noise reduction and IR detector performance in ways which have no precedent in older modes of IR detection. (For a more detailed discussion of this point see Appendix 1.)

The reason nonlinear dynamics concepts are so relevant to the detection mode under discussion here is that the process by which the detector generates a pulse is a highly nonlinear process.

6 Survivability of the Detectors Under High Incident Flux

There are many instances in which the possibility of exposure to high intensity IR sources could damage or have adverse effects on detectors or detector systems. Since the detectors under study exhibit an unusually high dynamic range, it is natural to think that such detectors might be unusually tolerant of abuse in the form of exposure to very high intensity radiation.

6.1 High Power Blackbody Exposures

Although not part of the original workplan, some preliminary measurements of survivability were made on a few devices near the end of Phase I. The results were very encouraging.

A few detectors of the type under study were tested with a heater very close to the detector. The pulse rate was measured using a hex scaler controlled through a CAMAC system connected to an IBM PC. See Fig. 10. The heater power was increased to about 20 watts. The pulse frequency went up to a point where the detector switched into a steady state conducting mode with no pulsing. In other words, pulsing gave way to a steady dc current. When the heater was switched off, the dc level came down to a point where the pulsing began again, indicating that the detector had survived. This process was repeated many times, but without any deterioration in performance.

7 Image Transfer without Multiplexing at the Focal Plane

We have performed a simple experiment in order to illustrate optical data transfer which could eliminate the need for multiplexing at focal plane. A p^+-n-n^+ diode drives a LED which is also inside the cryogenic environment. When the pulse from the p^+-n-n^+ diode goes above the threshold voltage of the LED, the LED starts conducting and emitting light. The LED firing pattern can be recorded using a CCD video camera. Fig. 11 shows a photograph of the firing LED inside the dewar taken from outside the dewar. While the p^+-n-n^+ diode pulse is greater than the LED threshold, the LED will be on and when the pulse is subthreshold the LED will switch off. The pulse will decay according to the circuit parameters, i.e. the time constant. The speed of data transfer will be limited by this RC time constant. The two curves in Fig. 13 show the waveforms for two different diodes. From these figures it is clear that the LED can be driven at kHz frequencies. A large LED array with each LED driven at kHz rates could provide high rate, fully parallel

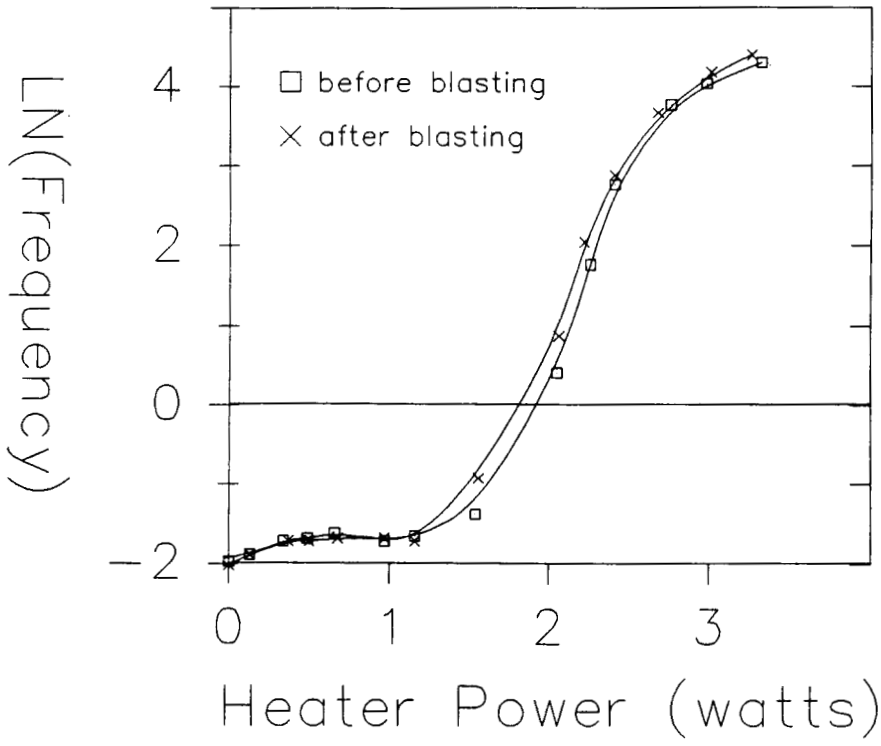

Figure 10: Pulse rate vs heater power before and after blasting the p^+-n-n^+ detector with 20 watts of heater power.

Figure 11: Photograph of an LED firing inside a dewar taken from outside the dewar through a plexiglass window. This illustrates a means of optical data transfer out of the cryogenic environment of an IR detector or imager. The outer ring is a reflection from the cylindrical tube supporting the LED. High resolution imaging of an LED array would permit very high rates of parallel data transfer with very low heat load.

transfer of IR image data out of the dewar. The data could be transferred to a processor or a multiplexer located outside the cryogenic environment.

8 Devices with Ultralow Power Requirements

It has been shown that very simple circuits containing a single p^+-n-n^+ diode can emulate many features of a real neuron[11] and could be used as building blocks for massive parallel asynchronous processors[20] and massive neural networks with very low power dissipation.[21] Von Neumann's estimate of the power consumption of the brain was 10-25 watts [22] which is remarkably small for a system with $\sim 10^{11}$ neurons, i.e. $\sim$ 100 picowatts/neuron. It has been argued that arrays of small p^+-n-n^+ diodes could offer comparably low (or even lower) power consumption.[21] For p^+-n-n^+ diodes, we have observed pulses with energy dissipation down to 4 picojoules/mm^2/pulse and a quiescent power dissipation of 10 picowatts/mm^2. Considering the thermodynamic efficiency of cooling, these numbers correspond to 290 picojoules/mm^2/pulse and 710 picowatts/mm^2 at room temperature. For comparison, we note that the retina chip of Mead and Mahowald[23] has a power dissipation of 4 microwatts/mm^2.

The range of p^+-n-n^+ diode pulse heights observed to date is from about 20 millivolts

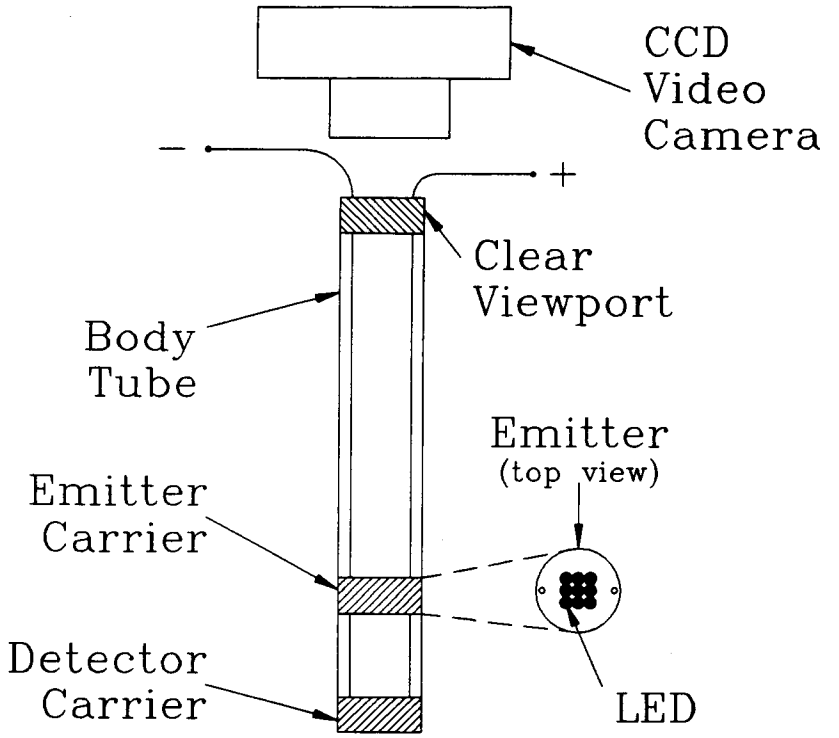

Figure 12: A schematic representation of the experimental setup showing the p^+-n-n^+ diode and the LED and the CCD video camera.

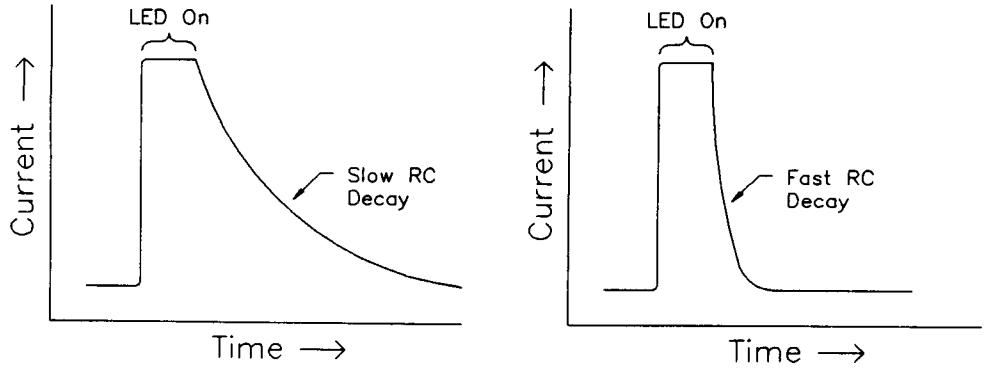

Figure 13: Left: Waveform showing the time interval during which the LED is on and the RC decay. Right: Waveform obtained for different circuit parameters showing the on region and the fast decay. Firing rates of up to a few kHz are possible with observed decay parameters.

to 50 volts with the low end of the range corresponding to the low power figures reported here. Massively parallel processors with ultralow power dissipation could be used just behind the focal plane to do image processing and data compression.[21] This would represent a considerable advance in infrared image processing.

9 Conclusion

The development of radiometric and imaging technology along the lines explored here would permit higher dynamic ranges than can be achieved with existing infrared systems. The pulse timing approach appears to possess fundamental advantages over approaches based on digitization of current, voltage or charge at the detector output. These advantages together with the low power consumption and the simplicity of the electronics should result in a competitive edge over older radiometry systems and imaging systems especially in connection with space-related applications and other cryogenic infrared system applications.

The possibility of incorporating photomultiplier effects is discussed in Appendix 3.

References

[1] B. T. Soifer, D. B. Sanders, B. F. Madore, G. Neugebauer, G. E. Danielson, J. H. Elias, C. J. Persson and W. L. Rice, *The IRAS Bright Galaxy Sample II. The Sample and Luminosity Function*, Infrared Processing and Analysis Center, IRAS Preprint No. 0026.

[2] M. Harwit, J. R. Houck, B. T. Soifer and G. G. C. Palumbo, *The Most Luminous Far-Infrared Extragalactic Sources*, Infrared Processing and Analysis Center, IRAS Preprint No. 0023.

[3] Edited by G. Burbidge, D. Layzer and J. G. Phillips, *Annual Review of Astronomy and Astrophysics-vol 24*, Annual Reviews Inc., California, 1986.

[4] D. D. Coon and A. G. U. Perera, Applied Physics Letters **51**, 1711 (1987).

[5] D. D. Coon and A. G. U. Perera, Solid-State Electronics **29**, 929 (1986).

[6] D. D. Coon and A. G. U. Perera, Int. J. Infrared and Millimeter Waves **7**, 1571 (1986).

[7] D. D. Coon, S. D. Gunapala, R. P. G. Karunasiri and H.-M. Muehlhoff, *An Integrating IR Detector* in **Infrared Technology IX,I. J. Spiro and R. A. Mollicone, Editors**, Proc. SPIE 430, 1983, pp. 144-151.

[8] D. D. Coon, S. D. Gunapala, R. P. G. Karunasiri and H.-M. Muehlhoff, International Journal of Infrared and Millimeter Waves **5**, 197 (1984).

[9] D. D. Coon, S. D. Gunapala, R. P. G. Karunasiri and H.-M. Muehlhoff, Electronics Letters **19**, 1070 (1983).

[10] D. D. Coon, S. D. Gunapala, R. P. G. Karunasiri and H.-M. Muehlhoff, *High Sensitivity Sampling IR Detector* in **Third International Conference on Infrared Physics, W. Ruegsegger and F. K. Kneubuhl ,Editors**, Proc.CIRP 3, 1984, pp. 359-361.

[11] D. D. Coon and A. G. U. Perera, Int. J. Electronics **63**, 61 (1987).

[12] D. D. Coon and A. G. U. Perera, Solid State Electronics **31**, 851 (1988).

[13] D. D. Coon, S. N. Ma and A. G. U. Perera, Phys. Rev. Lett. **58**, 1139 (1987).

[14] D. D. Coon and A. G. U. Perera, Applied Physics Letters **51**, 1086 (1987).

[15] N. F. Mott, *Metal-Insulator Transitions*, Barnes and Noble, New York, 1974.

[16] A. G. Milnes, *Deep Impurities in Semiconductors*, John Wiley & sons, N. Y, 1973, page 379.

[17] D. D. Coon and R. P. G. Karunasiri, Solid State Electronics **26**, 1151 (1983).

[18] Y. N. Yang, D. D. Coon and P. F. Shepard, Applied Physics Letters **45**, 752 (1984).

[19] S. B. Stetson, D. B. Reynolds, M. G. Stapelbroek, and R. L. Stermer, *Infrared Detectors, Sensors and Focal Plane Arrays*, SPIE 686, 48 (1986).

[20] D. D. Coon and A. G. U. Perera, Int. J. IR and Millimeter Waves **8**, 1037 (1987).

[21] D. D. Coon and A. G. U. Perera, *New Hardware for Massive Neural Networks* in **Neural Information Processing Systems**, American Institute of Physics, 1988, pp. 201–210.

[22] J. von Neumann, *Collected Works*, Pergamon Press, New York, 1961.

[23] C. A. Mead and M. A. Mahowald, Neural Networks **1**, 91 (1988).

[24] M. D. Petroff, M. G. Stapelbroek and W. A. Kleinhans, Appl. Phys. Lett. **51**, 406 (1987).

[25] M. G. Stapelbroek, M. D. Petroff, J. J. Speer and R. Bharat , *Origin of Excess Low-Frequency Noise at Intermediate Infrared Backgrounds in BIB Detectors*, Rockwell Preprint.

[26] K. M. S. V. Bandara, D.D. Coon and R. P. G. Karunasiri, Appl. Phys. Lett. **51**, 961 (1987).

APPENDIX 1

Mode-locked infrared sensor

D. D. Coon
Microtronics Associates, 4516 Henry Street, Pittsburgh, Pennsylvania 15213

A. G. U. Perera
Applied Technology Laboratory, Department of Physics, University of Pittsburgh, Pittsburgh, Pennsylvania 15260

(Received 20 February 1987; accepted for publication 11 August 1987)

Injection mode infrared detector concepts are expanded to incorporate the nonlinear dynamics concept of mode locking. The first successful demonstration of this approach is reported. The detectors employ extrinsic silicon and have large output signals which require no electronic amplification. Mode locking greatly reduces fluctuations in detector output without a corresponding reduction in detector responsivity. The results could lead to the development of a new class of sensors which exploit recent work on the distinction between deterministic fluctuations in nonlinear systems and intrinsic noise.

Previous work[1-4] has led to a class of infrared (IR) detectors, called injection mode detectors, with extraordinarily large output signals. The output consists of a series of pulses which are associated with temporarily switching of most of the dc bias voltage across the load impedance (see Fig. 1). No preamplifiers or amplifiers are necessary. The response to incident IR flux consists of changes in the rate and temporal pattern of pulsing. Thus, the device acts like a switch whose switching is controlled by IR illumination. The detector output can be characterized by a time series T_n with $n = 1,2,3,...$, where T_n represents the time intervals between successive pulses. The mode-locking effect reported here involves locking into a periodic pattern of pulsing such that T_n is a periodic function of n. Within the mode-locked regime, the pulse rate remains sensitive to changes in IR intensity and fluctuations in the pulse rate are small.

The detector is a silicon p^+-n-n^+ diode with substantial forward bias. Low-temperature operation and the presence of an impurity band offset at the n-n^+ interface inhibit injection. Large injection pulses are triggered by the buildup of an n-region space charge as a result of IR induced donor photoionization. The output waveform reflects the nonlinear dynamics in the device. Between pulses the detector integrates the IR signal. The mode of operation bears some similarity to integrate-and-fire models of nonlinear systems[5] and relaxation oscillators.[6]

For the detectors discussed here, electrical background noise is negligibly small compared to the size of the pulses. As a result, the relevant noise is contained within *fluctuations* in the time intervals between pulses. However, not all of the time interval fluctuations reflect noise. Recent work on nonlinear dynamics indicates that fluctuations in nonlinear systems can have a deterministic relationship to the parameters of the nonlinear system.[7,8] This suggests that for the devices under consideration, a sizeable component of the fluctuations in the temporal pattern could be deterministically related to parameters like IR intensity and bias voltage and unrelated to true performance-limiting noise.

The distinction between deterministic fluctuations and true noise, together with recently achieved understanding of nonlinear systems, could lead to significant advances in IR detector performance. Mathematical models of nonlinear systems provide some guidance and understanding in this area. Many of the models are formulated in terms of iterative maps. As an illustrative example, consider the iterative map: $T_{n+1} = f(T_n)$, where f is a nonlinear function which relates successive terms in a time series T_n with $n = 1,2,3,...$ The function f may involve a number of parameters whose values can dramatically affect the temporal pattern of the time series. For our system, two important parameters are IR intensity and bias voltage. Iterative maps can generate time series which range from periodic to chaotic even though the maps are deterministic. They thus provide a mathematical example of how fluctuations in time series might not represent noise. If time series information including deterministic fluctuations were fully utilized, and one had sufficient knowledge about f, one could pin down the parameters of f quite precisely. One can think of this as decoding the time series to obtain information about the parameters of the iterative mapping. The decoding problem is in some sense the inverse of the mapping problem. Since IR intensity is a sought after parameter and bias voltage is a known adjustable parameter, one can regard IR detection as a special type of decoding, or inverse mapping problem. In a region of parameter space where a mapping generates a chaotic time series, the decoding problem is difficult while in a periodic regime the decoding problem is simple. If an injection mode detector output is periodic with period P, i.e., $T_n = T_{n+P}$ for a range of IR intensities, then decoding simply involves empirical determination of the relationship between IR intensity and P successive time intervals.

In between the extremes of periodicity and chaos lie regimes of varying complexity. Small fluctuations are possible as are larger fluctuations and intermittancy. It is an especially interesting result of work on iterative maps, that even intermittancy can be understood as deterministic behavior.[9] From a detector point of view it seems most convenient to

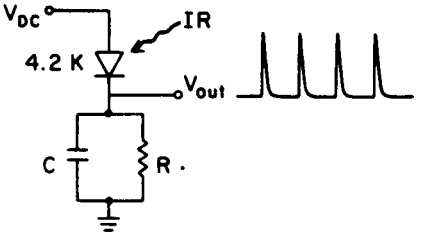

FIG. 1. Circuit diagram showing the IR detector at 4.2 K and an output pulse train.

 0003-6951/87/401086-03$01.00

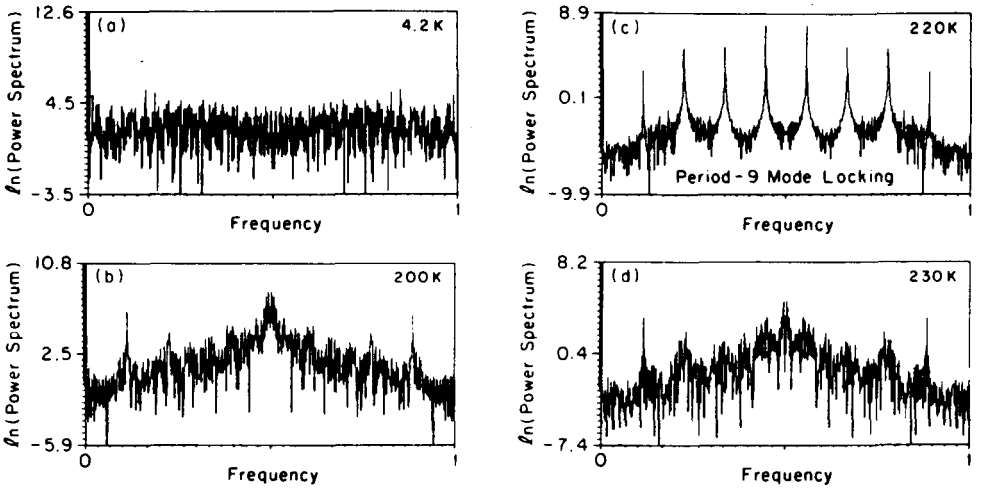

FIG. 2. Power spectra obtained from 1024 measured interpulse time intervals at 9.138 V bias for different blackbody source temperatures: (a) 4.2, (b) 200, (c) 220, and (d) 230 K. The vertical axis has a logarithmic scale. The frequency variable on the horizontal axis is the inverse of the time series periodicity.

work as closely possible to the simple periodic regime. Fortunately, work on iterative maps leads one to anticipate the existence of nearly periodic or mode-locked *regions* of parameter space. Extensive work has been done recently on mode locking and related phenomena in nonlinear systems.[10–16] Mode locking within certain ranges of the system parameters is a strong indication of deterministic behavior in nonlinear systems. The existence of narrow peaks in the injection mode detector power spectra reported here supports the view that injection mode detectors are deterministic systems. The power spectra are associated with Fourier transforms over the time series index n. Period P is associated with peaks at a frequency $1/P$ and harmonics thereof.

In Figs. 2 and 3, we see that as a function of IR source temperature, with a fixed bias voltage, an injection mode IR detector can pass through mode-locked regimes. The large, narrow peaks indicate closeness to the ideal situation of perfectly periodic, noise-free output. For a range of source temperatures, the detectors lock onto nearly periodic modes of pulsing. Figure 4 shows return maps which also indicate the nearly periodic behavior and display the fluctuations. From Fig. 4 we see that the 107 K data are more nearly periodic than the 102 K data. Similar mode-locking regions are observable as a function of bias voltage.

The simplest approach to detector readout is determination of IR induced changes in the average interpulse time interval. For example, in Fig. 2 the square root of the exponential of the zero frequency peak corresponds to the total time for 1024 pulses. Thus, changes in average time intervals as a function of the IR source temperature can be obtained from the power spectra. Simple averaging weights each time interval equally but it is by no means obvious that each interval has the same degree of fluctuation. This suggests that for nearly periodic behavior with period P, we weight each of the P subsets of the interpulse time series with a different weight. Notice that the weighted average approach only minimizes the effect of fluctuations and does not extract information from the deterministic component of the fluctuations. Thus, we do not expect this procedure to get us down to the level of true noise. However, weighted averaging is an approach which takes advantage of mode locking and it provides a baseline analysis.

The optimization problem for the weights consists of trying to minimize fluctuations subject to some constraint. The basic constraint is that one does not want to introduce weights which will appreciably reduce the weighted detector output signal, i.e., the weighted time series measure of the detector response to IR. The optimization problem can be

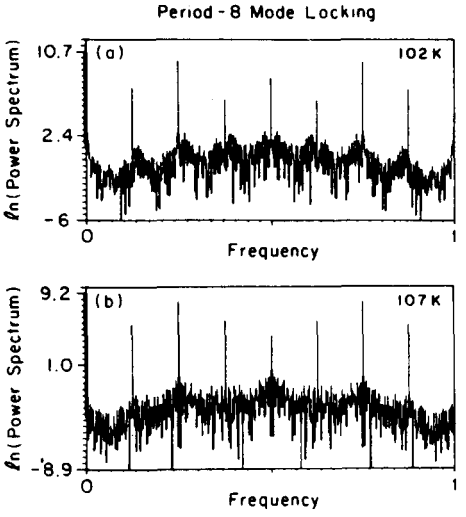

FIG. 3. Power spectra obtained from 1024 interpulse time intervals at 8.886 V for two different blackbody temperatures: (a) 102 and (b) 107 K.

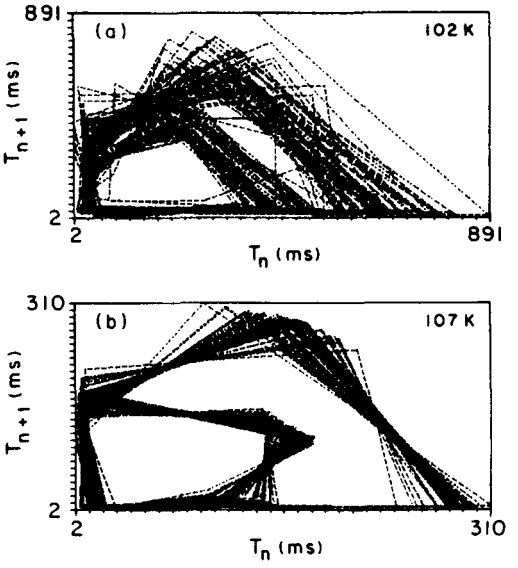

FIG. 4. Return maps for 500 measured interpulse time intervals at (a) 102 and (b) 107 K.

solved as follows. For period P we introduced a P-component vector to represent the P mean values associated with the P subsets of the interpulse time series: $\mathbf{A} = (A_1,...,A_P)$, with $A_m = \frac{1}{I}\sum_{i=1}^{I} t_{m+iP-P}$, (1)

where I is the number of periods in a time series with a total number IP of time intervals. For the ith period in an interpulse times series, we introduce a P-component vector representing the P interpulse time intervals in the ith period: $\mathbf{V}_i = (T_{iP-P+1}, T_{iP-P+2},..., T_{iP})$. We similarly introduce a vector representing P deviations in the ith period from the P means: $\mathbf{U}_i = \mathbf{V}_i - \mathbf{A}$. We introduce a dual P-component vector corresponding to the P weights of interest: $\boldsymbol{\epsilon} = (\epsilon_1,...,\epsilon_P)$. The weighted sum of deviations for the ith period of $\boldsymbol{\epsilon}\cdot\mathbf{U}_i$, where the dot product of the vectors indicates the usual contraction, i.e., summation over component indices. The mean square weighted deviation is

$$\frac{1}{I}\sum_{i=1}^{I} (\boldsymbol{\epsilon}\cdot\mathbf{U}_i)^2 = \boldsymbol{\epsilon}^T H \boldsymbol{\epsilon}, \quad (2)$$

where on the right-hand side $\boldsymbol{\epsilon}$ is regarded as a column vector, $\boldsymbol{\epsilon}^T$ as a row vector, and H is a P by P matrix.

In response to a small change in the infrared flux incident on the detector, the time series representing the detector output is still locked in a mode with periodicity P but the P-component vector representing the P mean values will change from $\mathbf{A}$ to some other P component vector $\mathbf{B}$. We therefore associate the detector response in terms of output signal with the vector $\mathbf{R} = \mathbf{B} - \mathbf{A}$ and the weighted response with $\boldsymbol{\epsilon}\cdot\mathbf{R}$. We next minimize the mean square weighted deviation subject to the constraint that the square of the weighted response remains fixed, i.e., $(\boldsymbol{\epsilon}\cdot\mathbf{R})^2 = \boldsymbol{\epsilon}^T G \boldsymbol{\epsilon} = c(\text{constant})$. Here we have taken the opportunity to define a response matrix G. Minimization leads to a modified eigenvalue problem

$$H\boldsymbol{\epsilon} = \gamma G \boldsymbol{\epsilon}, \quad (3)$$

with solutions for $\boldsymbol{\epsilon}$ being the P eigenvectors and γ entering as a Lagrange multiplier. The P eigenvalues of γ are the roots of $\det(H - \gamma G) = 0$.

We would next expect to vary c and find the value of c which minimizes the ratio of the mean square weighted deviation to the square of the weighted response. However, using Eq. (3) we see that this ratio is independent of c so no further minimization is necessary. Thus, we find that the lowest ratio of noise to response is just the square root of the lowest eigenvalue:

$$\frac{\text{noise}}{\text{response}} = \left(\frac{\boldsymbol{\epsilon}^T H \boldsymbol{\epsilon}}{\boldsymbol{\epsilon}^T G \boldsymbol{\epsilon}}\right)^{1/2} = (\gamma_{\min})^{1/2}. \quad (4)$$

This corresponds to the highest signal to noise ratio. Because the result involves an eigenvalue but no eigenvector, it allows one to compute the optimal noise to response ratio without actually computing any weighted averages.

In Fig. 3 we show data for a detector with two different IR source temperatures differing by 5 K. From the power spectra, periodicity 8 is obvious. From the time series data we form 8×8 matrices H and G with H being the fluctuation matrix at 107 K and G representing the detector response to the 5 K change. The lowest eigenvalue is $\gamma = 4\times 10^{-6}$ corresponding to a minimum resolvable temperature of 0.01 K. The corresponding value for unweighted averaging is 0.03 K.

In our work we noticed no hysteresis effect associated with the pulse rate in our system. We performed tests to check for hysteresis when the detector is mode locked. The detector bias and load were first chosen to produce mode locking without any IR incident on the detector (i.e., shutter closed). Then we compared the pulse rates with shutter positions: closed, open, closed. Next the detector was made to mode lock with incident IR (i.e., shutter open). Then the pulse rates were compared with the shutter positions: open, closed, open. From these measurements we conclude that if there is any hysteresis it is less than 0.02% i.e., output frequency difference as a fraction of output frequency. In theoretical studies, there is a critical line below which mode-locked regions do not overlap.[17] In this region one would not expect hysteresis.

The performance of the detector seems remarkably good especially when one considers that (a) there is no sensitive electronics associated with the readout, (b) the information content associated with the concept of deterministic fluctuations has not yet been exploited, (c) no survey has yet been performed to find the most favorable mode-locking regimes, and (d) no effort has been made to optimize response through adjustment of device parameters. The work indicates that the mode-locking strategy is feasible. Further work should address the tailoring of the mode-locking regime to particular ranges of IR source temperature or IR intensity, since optimal performance appears to correspond to centering the mode-locking regime on the range of interest. Additional work will address the determination of the fundamental inherent detector noise. The identification of an iterative mapping function which corresponds to the detector would be of help in developing an approach to separation of fundamental noise from deterministic fluctuations. One of the most important conclusions of the present work is that injection mode detectors show behavior like that discussed in work on deterministic nonlinear systems so that one can realistically expect further progress along the lines discussed here.

This work was supported by the U.S. Army under contract No. DASG60-86-C-0075. We are pleased to acknowledge helpful communication with P. Bak.

[1] D. D. Coon and S. D. Gunapala, J. Appl. Phys. **57**, 5525 (1985).
[2] D. D. Coon and A. G. U. Perera, Solid-State Electron. **29**, 929 (1986).
[3] L. H. De Vaux, U. S. Patent No. 3 466 448.
[4] D. D. Coon and A. G. U. Perera, Int. J. Infrared Millimeter Waves 7, 1571 (1986).
[5] B. W. Knight, J. Gen. Physiol. **59**, 734 (1972).
[6] L. O. Chua, *Introduction to Nonlinear Network Theory* (McGraw-Hill, New York, 1969).
[7] R. M. May, Nature **216**, 459 (1976).
[8] G. Mayer-Kress, ed., *Dimensions and Entropies in Chaotic Systems* (Springer, New York, 1986).
[9] J. Hirsch, B. Huberman, and D. Scalapino, Phys. Rev. A **25**, 519 (1982).
[10] P. Bak, T. Bohr, and M. H. Jensen, Phys. Scr. **T9**, 50 (1985).
[11] P. Cvitanovic, M. H. Jensen, L. P. Kadanoff, and I. Procaccia, Phys. Rev. Lett. **55**, 343 (1985).
[12] L. Glass and R. Perez, Phys. Rev. Lett. **48**, 1772 (1982).
[13] M. H. Jensen, P. Bak, and T. Bohr, Phys. Rev. Lett. **50**, 1637 (1983).
[14] M. R. Guevara, L. Glass, and A. Shrier, Science **214**, 1350 (1981).
[15] M. Feigenbaum, "Renormalization of the Farey Map and Universal Mode Locking" (unpublished).
[16] D. D. Coon, S. N. Ma, and A. G. U. Perera, Phys. Rev. Lett. **58**, 1139 (1987).
[17] T. Bohr, P. Bak, and M. H. Jensen, Phys. Rev. A **30**, 1970 (1984).

Infrared transient sensing

D. D. Coon, MEMBER SPIE
R. P. G. Karunasiri*
Microtronics Associates
4516 Henry Street
Pittsburgh, Pennsylvania 15213

K. M. S. V. Bandara
University of Pittsburgh
Department of Physics
Applied Technology Laboratory
Pittsburgh, Pennsylvania 15260

Abstract. An experiment has been carried out to show that extrinsic silicon injection-mode infrared detectors can be used to simulate the transient response of neurons in biological vision systems. The neural response provides a means of high pass filtering in vision system focal plane parallel processing. The high pass filtering emphasizes transients in images. Possible IR imaging applications include surveillance, motion sensing, and tracking. The IR detector output pulses are sufficiently large that amplification is not required. This could facilitate parallel processing in or near the focal plane. The IR transient sensing approach is quantitatively analyzed in terms of a model for the detector and the associated circuitry. Excellent agreement is found between the model and the experimental data.

Subject terms: infrared; infrared transient sensing; silicon detectors; vision systems; focal plane processing.

Optical Engineering 27(6), 471-474 (June 1988).

CONTENTS

1. INTRODUCTION

The present work demonstrates the use of injection-mode infrared detectors to simulate a key feature of biological vision systems. Biological vision systems perform many functions much better than do conventional optoelectronic imaging arrays coupled to standard readout systems. Vision systems seem especially well suited to the performance of complex tasks such as tracking a set of objects moving against background clutter.[1-3] They incorporate a high degree of parallel processing,[4] part of which occurs at or near the focal plane. In IR imaging systems utilizing conventional IR detectors, fully parallel processing would require one preamplifier for every detector in a two-dimensional array. This would add prohibitive complexity to large arrays. The IR detector employed in the present work requires no preamplifiers, so a high degree of parallel processing is possible. Another feature of the detector considered here is that its output consists of neuronlike spiketrains. This feature could facilitate a neural network approach to processing.[5] This may be of special interest because of the current surge of interest in neural network processing. Neuronlike behavior has been simulated with circuits,[6,7] but our approach is based more on a specific physical device than a circuit. In other words, the neuronlike dynamics is related to device physics. No transistors are employed. This fact distinguishes our approach from all other electronic approaches of which we are aware. Arrays of devices and networks employing devices and concepts discussed herein can be constructed. In this way, spatial receptive fields could be formed.

Spiketrain coding is potentially very useful for high dynamic range coding of signals in dense networks, where crosstalk and noise could cause problems with conventional analog (amplitude-modulated) signal transmission. Frequency modulation rather than amplitude modulation is the basis of spiketrain information coding.

2. SELF-INHIBITION

One aspect of focal plane processing in vision systems involves the response to transient features in images. This is important for tracking, motion sensing, and fast reaction to sudden changes in a fixed scene. Visual system response to

*Current affiliation: Device Research Laboratory, Department of Electrical Engineering, University of California at Los Angeles.

Paper 2390 received March 5, 1987; revised manuscript received Feb. 1, 1988; accepted for publication Feb. 11, 1988; received by Managing Editor Feb. 16, 1988.

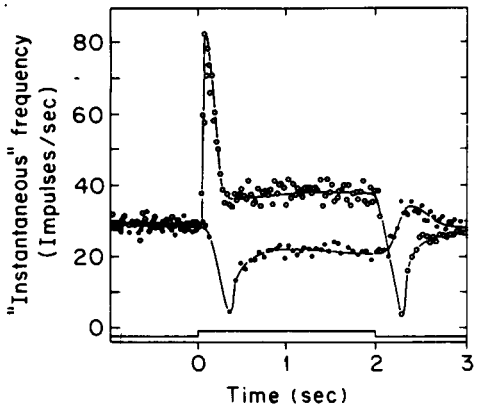

Fig. 1. Instantaneous frequency response of two adjacent receptor units in the lateral eye of *Limulus* to the step increment of illumination as shown by the signal at the bottom of the figure.[8] The upper and lower curves show excitatory and inhibitory responses, respectively.

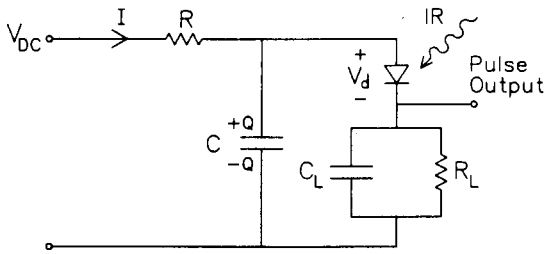

Fig. 2. Diagram of the circuit that converts IR intensity to a spiketrain output. C_L and R_L constitute the load impedance.

transients involves self-inhibition or rapid adaptation. Figure 1 presents data for simultaneous excitatory and inhibitory transients in two adjacent receptor units in the lateral eye of *Limulus*.[8] The role of self-inhibition is to suppress the response to slow changes in the optical input. Because there is a time delay associated with self-inhibition, sudden changes in optical input are not suppressed. Self-inhibition thus constitutes a form of processing that emphasizes transients. This processing can be carried out at the level of individual neurons in vision systems or at the level of individual detector elements in the work described here. One can regard this processing as a form of filtering that operates specifically with neuronlike spiketrains. Self-inhibition can be thought of as a negative feedback effect in which an increase in the firing rate of a neuron causes a subsequent partially compensating decrease in the neuron's own firing rate.

In place of a neuron, we employ a silicon p^+-n-n^+ diode with a substantial forward bias. Normal injection is hindered by low temperature operation and the presence of impurity band offsets at the n-n^+ and the p^+-n interfaces. Neuronlike firing involves large injection pulses associated with temporary switching of the diode into an on state. The diode is switched off by a drop in the potential across the diode. This is caused by an increase in the potential across a load impedance (see Fig. 2). Exposure of the diode to IR radiation induces changes in the firing rate. The diode when operated in the mode just described is referred to as an injection-mode IR detector.[9–12]

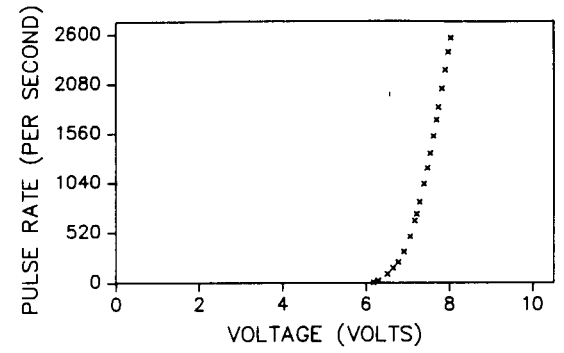

Fig. 3. Pulse rate versus bias voltage across the diode without IR illumination. Circuit parameters are R = 19.6 kΩ, C = 547 μF, R_L = 1 kΩ, and C_L = 20 nF.

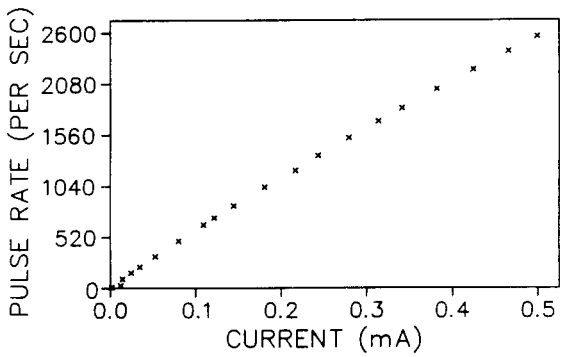

Fig. 4. Pulse rate versus current through the diode without IR illumination. Circuit parameters are the same as in Fig. 3.

3. DETECTOR CIRCUIT AND DATA ANALYSIS

The circuit in Fig. 2 implements self-inhibition for injection-mode IR detectors. The ideas behind the circuit are as follows. The diode is normally off, i.e., in a nonconducting state. In this state, the voltage across the diode V_d is equal to V_C, the voltage across a larger capacitance C. Each time the diode fires, it accomplishes a fast transfer of charge from C onto the smaller load capacitor C_L. The charge transferred times the frequency of firing (switching) represents a current drain from the capacitor C. An approximate equilibrium is reached between the charge-transfer rate and a recharging current through the resistor R. There is an abrupt increase in the firing (switching) rate of the diode for V_C near the firing threshold V_T (see Fig. 3). This nonlinear behavior of the firing rate near threshold tends to pin V_C to a value near V_T. This results in approximately the same amount of charge being transferred each time the diode fires, giving a linear relationship between frequency and the current through the resistor R (see Fig. 4). Exposure to IR radiation changes the firing rate of the diode. An increase in the firing rate tends to discharge C and leads to a slight reduction in V_C. This reduction in V_C leads to a partially compensating (self-inhibiting) reduction in the firing rate. Similarly, a decrease in the firing rate leads to an increase in V_C and a partially compensating increase in the firing rate. For the diodes used in the present work, exposure to IR was found to cause increases or decreases in the firing rate depending on the bias voltage. Both increases and decreases in illumination-induced firing rate are found in biological vision systems.

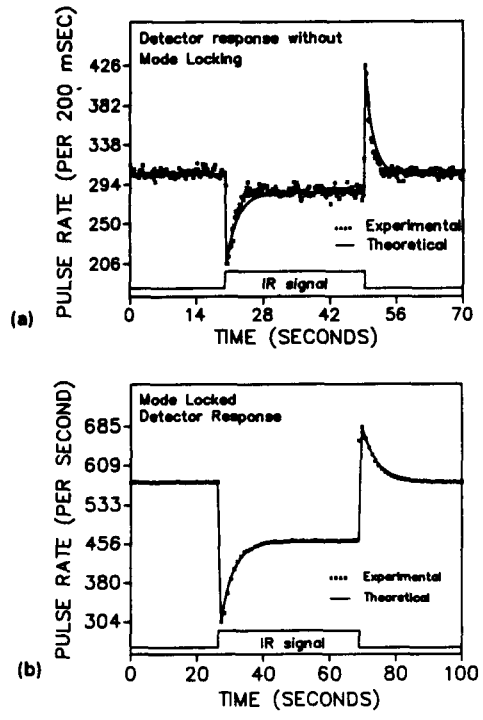

Fig. 5. Change in firing rate of the p-i-n diode with IR illumination that is first abruptly increased and then abruptly decreased, as indicated by the signal at the bottom of the figures. (a) Without mode locking. Circuit parameters are R = 7.3 MΩ, C = 9.8 μF, R_L = 11.7 kΩ, C_L = 220 pF, and V_{DC} = 7.5 V. The IR source temperature is T = 125 K. (b) Circuit parameters adjusted to operate the diode in the mode-locking region with period 1. R = 19.6 kΩ, C = 547 μF, R_L = 10 kΩ, C_L = 20 nF, V_{DC} = 8.0 V, and T = 100 K.

A microcomputer-controlled computer-automated measurement and control (CAMAC) data acquisition system was used to measure the firing rate of the diode as a function of time. Data were taken with a latching counter and a clock generator module. This provided direct measurement of the firing rate in terms of the clock generator time intervals. In Fig. 5, we show experimental data obtained with the circuit of Fig. 2.

The data in Fig. 5 show good agreement with theoretical curves obtained by the considerations described below. The theoretical results are useful in determining circuit parameters to tailor the shape of response curves to particular applications. Another aspect of circuit parameter selection is that for ranges of circuit parameters, mode locking[13–16] appears in the firing pattern of the detector. Thus, circuit parameters can be used to obtain periodic patterns with only small fluctuations in the interpulse time intervals. The difference in the amount of fluctuation associated with mode locking is apparent in Fig. 5.

An equation for the circuit shown in Fig. 2 can be written as

$$V_{DC} = IR + \frac{Q}{C}, \tag{1}$$

where I is the average current being drawn from the source. I can be written as the rate of change of charge on the capacitor C plus the rate at which charge is switched onto the capacitor C_L by the diode. If at the end of each firing the voltage across the diode is V_d, then the amount of charge transferred to the capacitor C_L is $(Q/C - V_d)\,C_L$. If the firing rate is F, then

$$I = \frac{dQ}{dt} + \left(\frac{Q}{C} - V_d\right)C_L F. \tag{2}$$

From Eqs. (1) and (2) we get

$$\frac{dQ}{dt} = -(1 + RC_L F)\frac{Q}{RC} + (V_{DC} + RC_L V_d F)\frac{1}{R}. \tag{3}$$

The firing rate of the diode is dependent on V_C and the effect of incident IR radiation. We found experimentally (see Fig. 3) that for a range of frequencies, F can be written to a good approximation in terms of V_C as

$$F = \alpha(V_C - V_T) + F_{IR}, \tag{4}$$

where α is a constant, V_T is the firing threshold as defined above, and F_{IR} is the contribution due to IR radiation incident on the diode. Substituting for V_C (= Q/C) and taking P as 1 + $RC_L F$, we find that Eq. (3) can be written as

$$RC\frac{dP}{dt} = -[P^2 - (P_{IR} - P_T)P - P_{DC}], \tag{5}$$

where $P_T = \alpha RC_L(V_T - V_d)$ and $P_{DC} = \alpha RC_L(V_{DC} - V_d)$. If there is an abrupt increase in IR intensity at time t = 0, then the firing rate of the diode will evolve according to Eq. (5).

By factoring the right-hand side of Eq. (5), we get

$$RC\frac{dP}{dt} = -(P - P_1)(P - P_2), \tag{6}$$

where P_1 and P_2 are given by

$$P_1 = \frac{(P_{IR} - P_T) + [(P_{IR} - P_T)^2 + 4P_{DC}]^{1/2}}{2},$$
$$P_2 = \frac{(P_{IR} - P_T) - [(P_{IR} - P_T)^2 + 4P_{DC}]^{1/2}}{2}. \tag{7}$$

If $P = P_0$ for $t < 0$, then for $t > 0$ the quantity P can be obtained by integrating Eq. (6) as

$$P = P_1 + \frac{(P_1 - P_2)}{\dfrac{(P_0 + P_{IR} - 1 - P_2)}{(P_0 + P_{IR} - 1 - P_1)}\exp\left[\dfrac{(P_1 - P_2)t}{RC}\right] - 1}. \tag{8}$$

Then, as a function of time, F is given by the quantity $(P - 1)/RC_L$. To compare with experiment, we obtained P_1 and P_2 using steady-state values of P before and after IR illumination and obtained P_{IR} from F_{IR}. The result, shown in Fig. 5, indicates that Eq. (8) provides a good description of the experimental data.

4. CONCLUSION

The successful implementation of self-inhibition with the injection-mode IR detector reported here indicates that focal plane processing for arrays of injection-mode detectors could employ self-inhibition to obtain useful transient response. The results also show that the approach to IR transient sensing described here can benefit from a reduction in detector output fluctuations associated with mode locking.

The equations that describe the operation of the circuit give a good description of the experimentally observed response.

Thus, they could be used for design purposes or to predict firing rates and rates of decay of firing rates in terms of particular device and circuit parameters.

5. ACKNOWLEDGMENT

This work was supported by the U.S. Army under contract DASG60-86-C-0075.

6. REFERENCES

1. K. Nakayama, "Biological image motion processing: a review," Vision Res. 25, 625 (1985).
2. R. P. Virsik and W. Reichardt, "Detection and tracking of moving objects by the fly musca domestica," Biol. Cybern. 23, 83 (1976).
3. W. Reichardt and T. Poggio, "Figure-ground discrimination by relative movement in the visual system of the fly," Biol. Cybern. 35, 81 (1979).
4. J. Stone, *Parallel Processing in the Visual System*, Plenum Press, New York (1983).
5. D. D. Coon and A. G. U. Perera, "Semiconductor electronic concepts for neural network emulation," Int. J. Electron. 63, 61 (1987).
6. L. D. Harmon, "Artificial neuron," Science 129, 962 (1959).
7. L. D. Harmon, "Studies with artificial neurons: properties and function of an artificial neuron," Kybernetik 1, 89 (1961).
8. F. Ratliff, H. K. Hartline, and W. H. Miller, "Spatial and temporal aspects of retinal inhibitory interaction," J. Opt. Soc. Am. 53, 110 (1963).
9. D. D. Coon and S. D. Gunapala, "New injection mode infrared detector," J. Appl. Phys. 57, 5525 (1985).
10. D. D. Coon and A. G. U. Perera, "Spectral response of an injection-mode infrared detector," Solid-State Electron. 29, 929 (1986).
11. D. D. Coon and A. G. U. Perera, "Spectral information coding by infrared photoreceptors," Int. J. Infrared and Millimeter Waves 7, 1571 (1986).
12. L. H. De Vaux, "Double injection photodetector having n^+-p-p^+," U.S. Patent 3466448 (1969).
13. P. Bak, T. Bohr, and M. H. Jensen, "Mode-locking and the transition to chaos in dissipative systems," Physica Scripta T9, 50 (1985).
14. P. Cvitanović, M. H. Jensen, L. P. Kadanoff, and I. Procaccia, "Renormalization, unstable manifolds, and the fractal structure of mode locking," Phys. Rev. Lett. 55, 343 (1985).
15. L. Glass and R. Perez, "Fine structure of phase locking," Phys. Rev. Lett. 48, 1772 (1982).
16. M. R. Guevara, L. Glass, and A. Shrier, "Phase locking, period-doubling," Science 214, 1350 (1981).

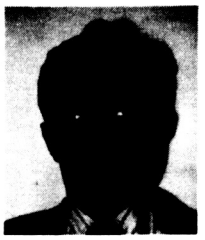

Darryl D. Coon is a professor of physics at the University of Pittsburgh and founder of Microtronics Associates. Coon's Ph.D. degree from Princeton University was in theoretical elementary particle physics and his research from 1967 to 1978 was mainly in that area. From 1978 until the present, his research has been mainly in semiconductor physics and devices, including extrinsic silicon and quantum well structures. Tunneling, infrared, ionizing radiation, electronic phenomena, neural networks, and new device concepts have been central features of this research. Coon is the author or coauthor of 80 publications in scientific and technical journals. Three patents relating to semiconductor devices have been awarded to Coon and coworkers.

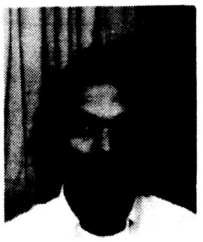

R. P. G. Karunasiri received his BS degree in physics from the University of Colombo, Sri Lanka, in 1979 and his Ph.D. degree in physics from the University of Pittsburgh in 1984. He was a research associate at Microtronics Associates in Pittsburgh from 1985 to 1987. He is currently employed at the University of California, Los Angeles, as a postgraduate research engineer. Current interests include IR detection using quantum wells and superlattices, computer-controlled data acquisition systems, and thin-film growth using molecular beam epitaxy.

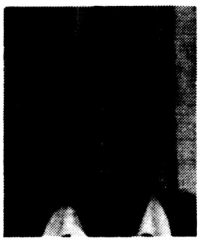

K. M. S. V. Bandara graduated from the University of Peradeniya, Sri Lanka, in 1981 with a B.Sc. degree in physics. He then completed a master's degree in physics at the University of Pittsburgh, where he is currently working in the field of quantum wells for his Ph.D. degree.

APPENDIX 3 - OTHER INFRARED RESEARCH BASED ON EXTRINSIC SILICON DEVICES

In this appendix, we show for comparison, some data on silicon impurity band infrared detection and single IR photon detection. See Figs. A-1 to A-6. This is motivated in part by work at Rockwell.[24,25] If we think of such detectors as current sources, then one can develop a strategy for performing photocurrent-to-frequency conversion using p^+-n-n^+ devices.[26] That approach has some merit, but differs from our Phase I research effort. Instead of using a detector to generate a photocurrent and then doing current-to-frequency conversion, the Phase I research involved **direct** intensity-to-frequency conversion. However, it would be desirable to see if some effects like gain, in the case of single photon detection, could be incorporated into the direct intensity-to-frequency conversion approach. *A priori*, this seems possible because all of the devices discussed here and in connection with our Phase I research are extrinsic silicon devices. In particular, the devices used for single photon detection in the figures presented here are p-i-n structures which are very similar to the devices used in the research described in the report.

APPENDIX 3
FIG. A–1

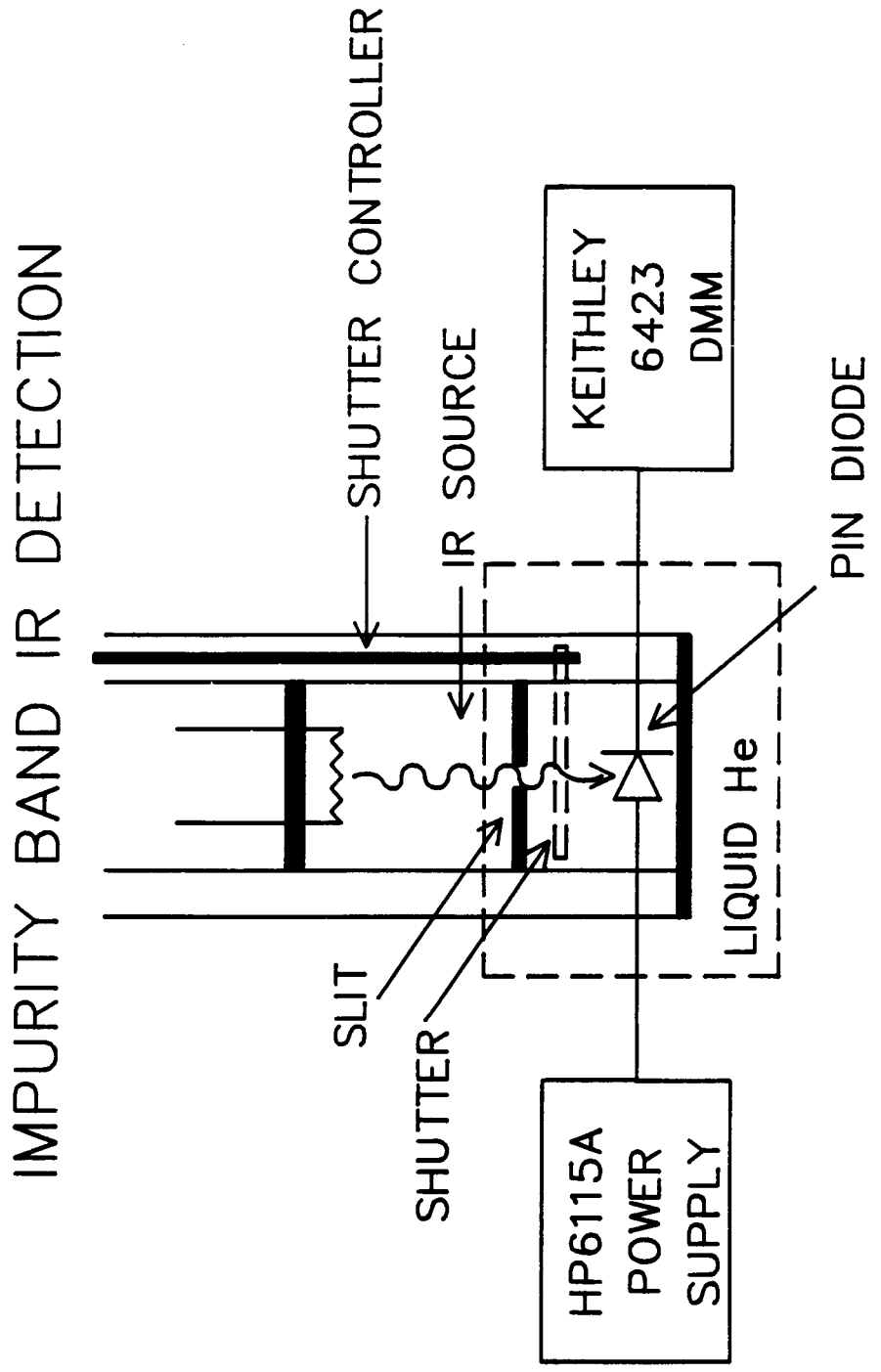

Experimental set up for impurity band IR photocurrent measurements. IR illumination on the diode is controlled by the shutter.

APPENDIX 3
FIG. A–2

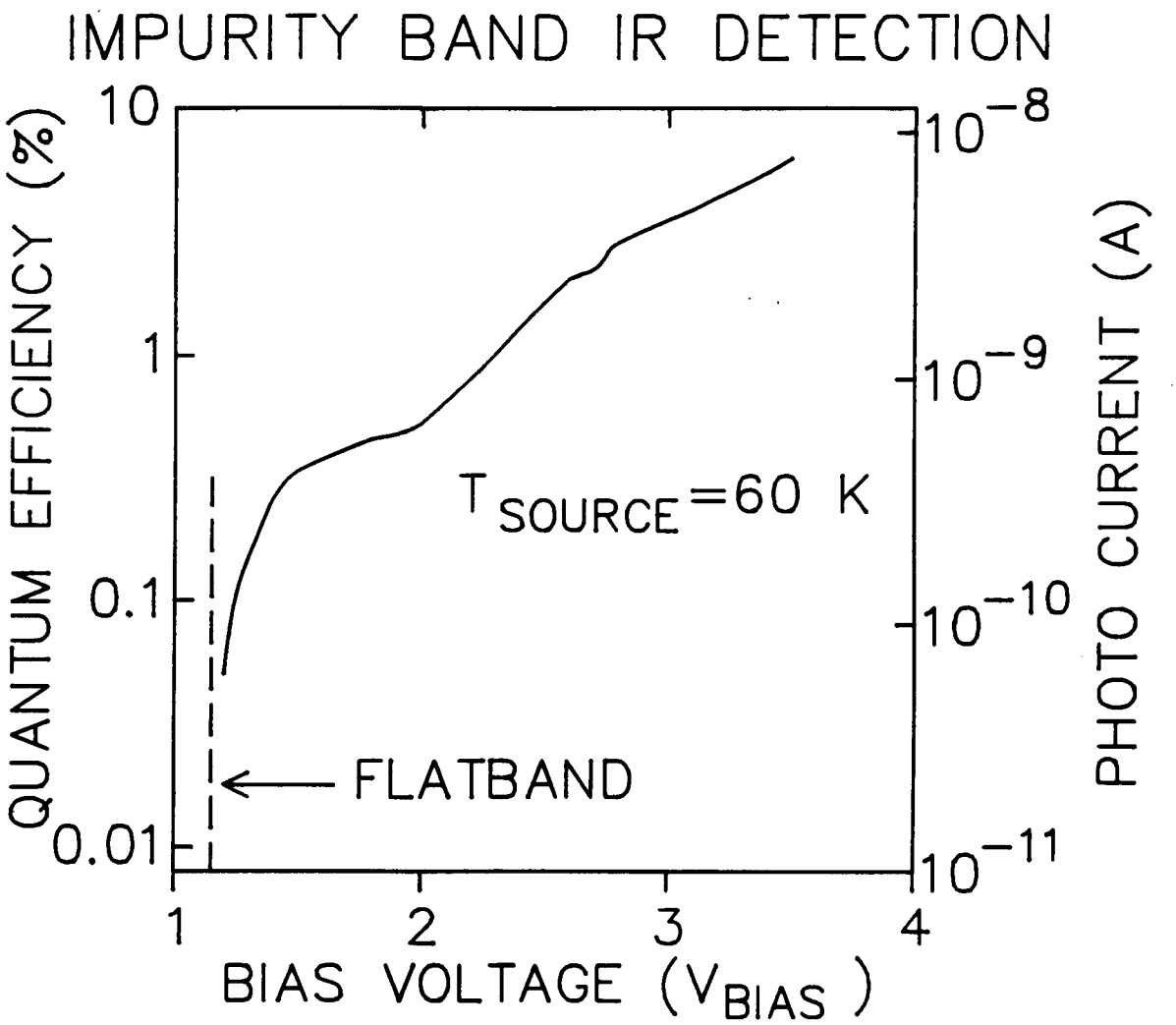

Experimental infrared photocurrent and quantum efficiency vs bias voltage for a forward biased p-i-n diode with area 1 mm^2. The detection mode involves impurity band effects. At V_{BIAS}=1.15 V, quantum efficiency drops sharply due to the flat band condition. The diode was illuminated with IR from black body source with a temperature 60K.

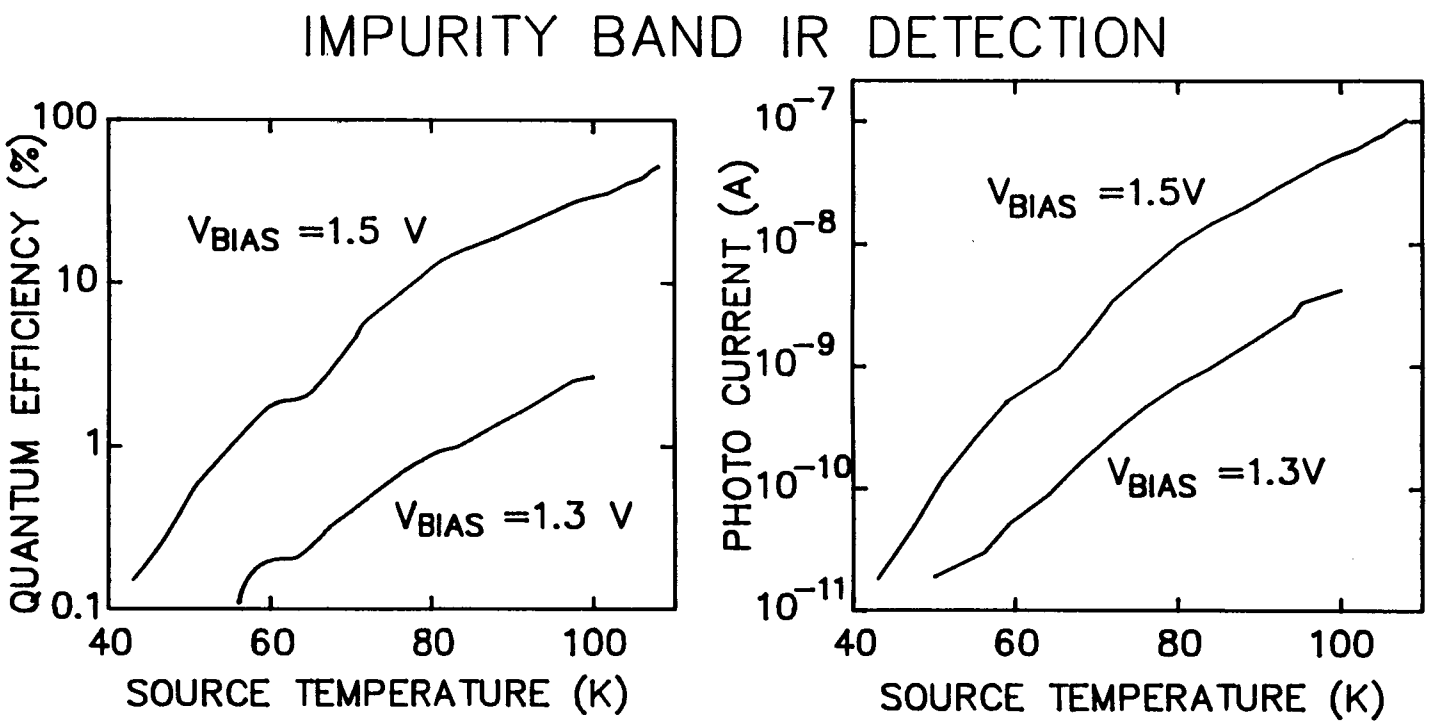

Experimental infrared photocurrent and quantum efficiency vs IR black body source temperature for a forward biased p-i-n diode with area 0.2 mm^2 at bias voltages V_{BIAS}=1.5V and V_{BIAS}=1.3 V.

APPENDIX 3
FIG. A-3

INTERFACING OF AN IMPURITY BAND IR DETECTOR TO THE FIRST STAGE OF A PARALLEL ASYNCHRONOUS PROCESSOR

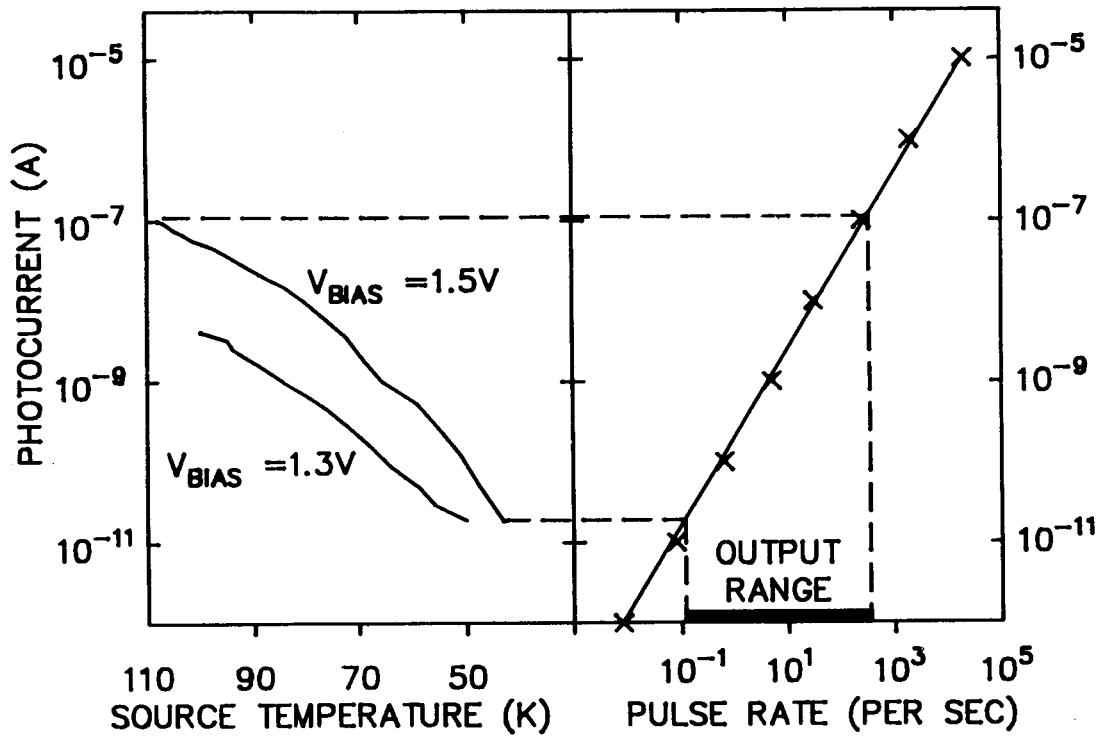

The graphs show that the photocurrent output a particular impurity band IR detector (left graph) falls within the dynamic range of p^+-n-n^+ devices (right graph). This implies that the impurity band IR detectors could be directly interfaced to a parallel asynchronous processor based on p^+-n-n^+ devices.

APPENDIX 3
FIG. A—4

APPENDIX 3
FIG. A–5

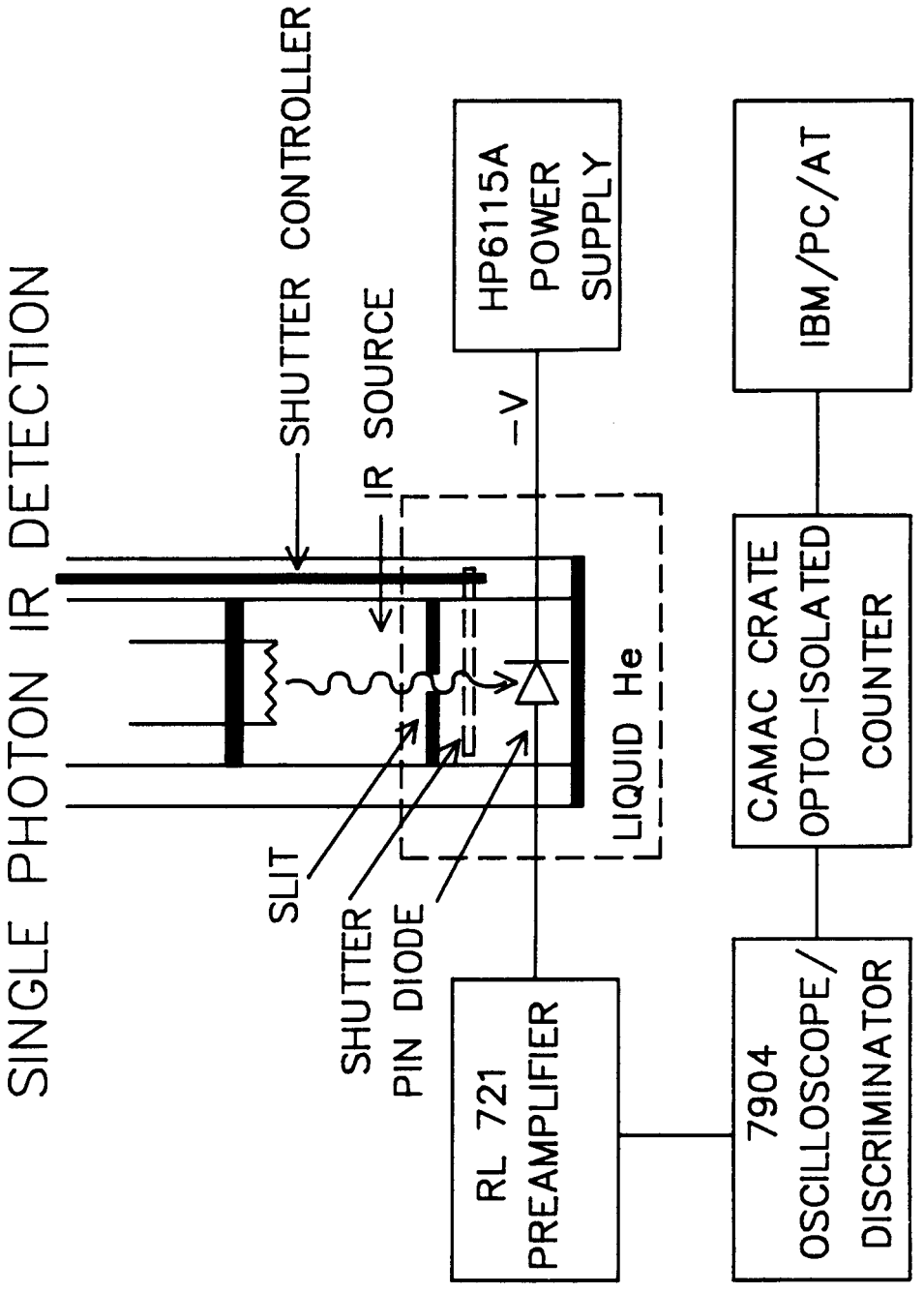

Experimental set up used to measure single photon IR detection. IR illumination on the diode is controlled by the shutter.

SINGLE PHOTON IR DETECTION

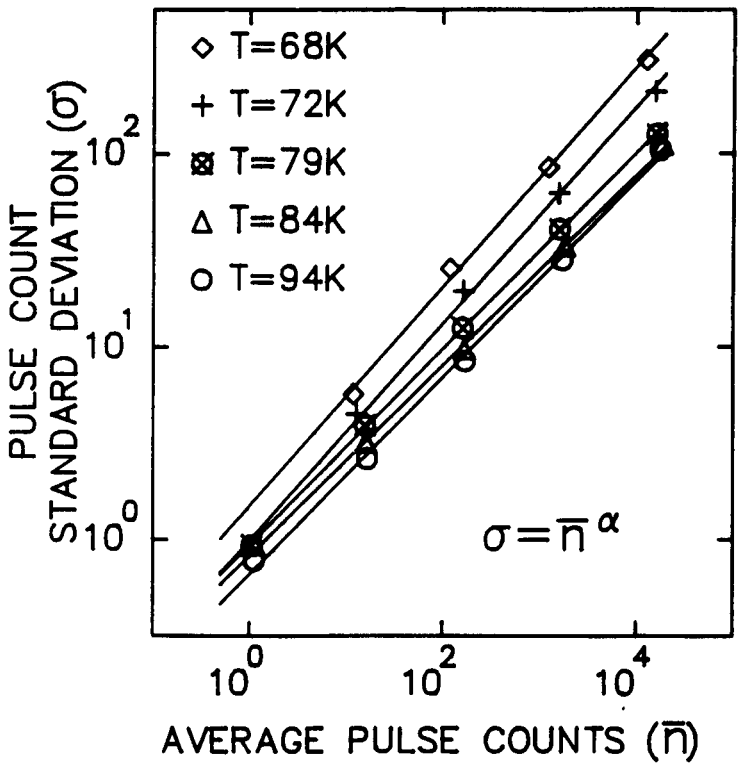

SOURCE TEMPERATURE	SLOPE (α)	INTERCEPT (C)
68K	0.57	1.5
72K	0.56	1.0
79K	0.51	0.94
84K	0.49	0.83
94K	0.51	0.67
POISSON STATISTICS	0.50	1.0

Standard deviation (σ) of the number of pulse counts vs the average number of pulse counts ($\bar{n}$). Numbers of counts were measured for different time intervals. Each line represents a fit to different black body source temperature data. Slopes (α) and intercepts (c) were obtained from least square fits to each set of points.